$Dn\#1356$

MASTER

Reactivity from Power Spectral Density Measurements with ^{252}Cf

J. T. Mihalczo
V. K. Paré
G. L. Ragan
M. V. Mathis
G. C. Tillet

OAK RIDGE NATIONAL LABORATORY

DISCLAIMER

DISCLAIMER

Portions of this document may be illegible in electronic image products. Images are produced from the best available original document.

ORNL/TM-5475
Dist. Category UC-79,
-79d, -79e, -79m, and
-79p

Contract No. W-7405-eng-26

INSTRUMENTATION AND CONTROLS DIVISION

REACTIVITY FROM POWER SPECTRAL DENSITY
MEASUREMENTS WITH ^{252}Cf

J. T. Mihalczo, V. K. Paré, G. L. Ragan,
M. V. Mathis, and G. C. Tillett*

Date Published: August 1977

NOTICE This document contains information of
preliminary nature. It is subject to revision
or correction and therefore does not represent
a final report.

Oak Ridge National Laboratory
Oak Ridge, Tennessee 37830
operated by
UNION CARBIDE CORPORATION
for the
ENERGY RESEARCH AND DEVELOPMENT ADMINISTRATION

THIS PAGE

WAS INTENTIONALLY

LEFT BLANK

ABSTRACT

The theory of a method of determination of the reactivity from power spectral density measurements with ^{252}Cf and the results of experiments with a critical assembly mock-up of a liquid-metal fast breeder reactor and with uranium (93.2 wt % ^{235}U) metal cylinders and a sphere are presented. This method of reactivity determination has an advantage over existing methods in that it determines the reactivity only from properties of the reactor at the subcritical state of interest and thus does not require a calibration near delayed criticality. In these experiments the reactivity was varied by changing the fissile loading or the amount of neutron absorber inserted; for the LMFBR mock-up, the reactivity varied to ~75 dollars subcritical, and for the uranium metal assemblies, to ~30 dollars subcritical. These experiments verified for the first time the predictions of theory that could be tested in the measurements. This method has potential use in the initial startup of LMFBRs or other fast reactors to determine the reactivity far subcritical before initial criticality is achieved. It has the advantage of not requiring a calibration by another method; furthermore, the interpretation of the measured data to obtain the reactivity does not depend on relative or absolute values of the source intensity or detection efficiency. It also can be used to determine the reactivity of assemblies where loading to criticality is undesirable or where sufficient material to achieve criticality is not available.

THIS PAGE

WAS INTENTIONALLY

LEFT BLANK

ACKNOWLEDGEMENTS

THIS PAGE

WAS INTENTIONALLY

LEFT BLANK

CONTENTS

1. INTRODUCTION

The theory of a method of determination of the reactivity from power spectral density measurements with ^{252}Cf[1-4] was tested in experiments[5-7] with a critical assembly mock-up of a liquid-metal fast breeder reactor (LMFBR) and with uranium metal cylinders and a sphere. This method determines the reactivity from properties of the reactor at the subcritical state of interest and, thus, does not require calibration near delayed criticality. This paper presents the methods of determining the reactivity from power spectral density measurements and shows how the various predictions of the theory have been verified by the experiments. In these experiments the reactivity was varied by changing the fissile loading or the amount of neutron absorber inserted; for the LMFBR mock-up, reactivity varied to ~75 dollars (k ≈ 0.8) subcritical; and for the uranium metal assemblies, to ~30 dollars subcritical (k ≈ 0.8).

2. THEORY OF REACTIVITY DETERMINATION FROM SPECTRAL DENSITY MEASUREMENTS

2.1 Description of the Method

To review the theory for this proposed measurement technique and compare the results with those from a two-detector cross-power spectral density (CPSD) measurement, consider a reactor with three detectors inserted in the core: a fission chamber which contains a spontaneous fission isotope, ^{252}Cf (detector 1); and a pair (2 and 3) that detect neutrons. A schematic diagram of the system for frequency domain measurement is shown in Fig. 1. The pair of detectors (2 and 3) detect neutrons emitted by fission chains initiated by neutrons from the spontaneous fission of the inherent source, and from the spontaneous fission of ^{252}Cf or by delayed neutrons. The neutron-induced fission rate in the chamber with ^{252}Cf is negligible compared with the spontaneous fission rate of ^{252}Cf for fluxes attainable in reactors. Thus the role of the ^{252}Cf chamber is to serve as a source of neutron noise for the reactor and--in its capacity as a detector--to provide a highly correlated
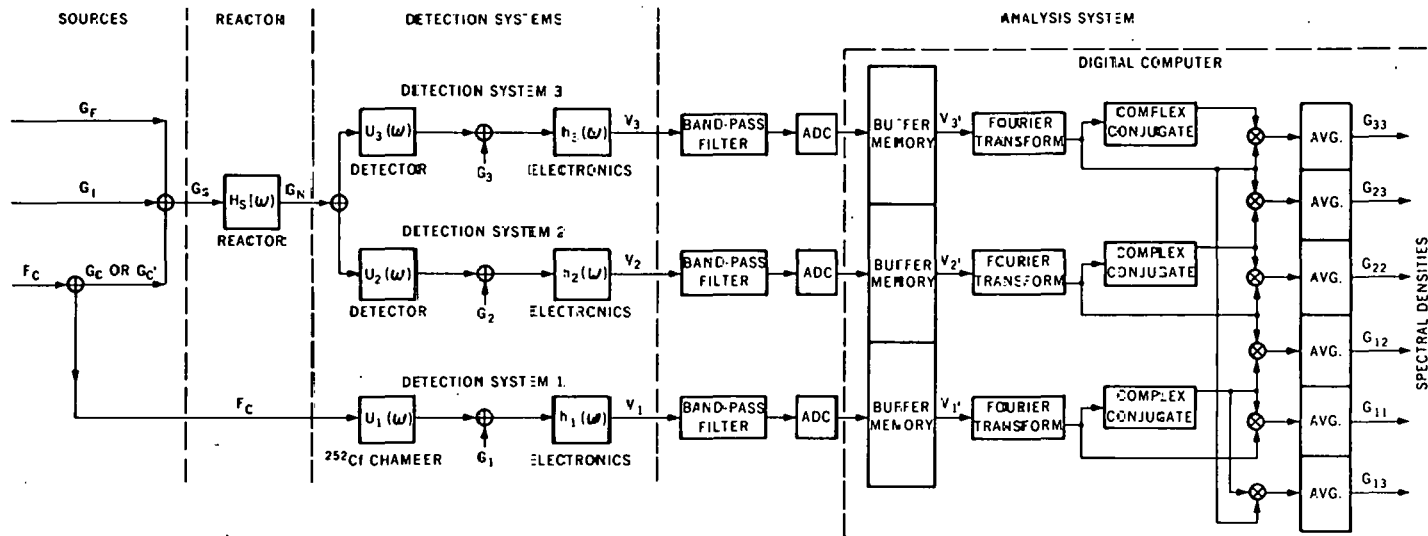
Fig. 1. Schematic diagram of correlation experiment with ^{252}Cf.

electrical representation of that noise for use in the analysis. The detectors may be operated in either the pulse or current modes; in any case the signals from all of them are conditioned by the electronics so that the output voltages V_1, V_2, and V_3 are proportional to the neutron interaction rates in the respective detectors. This proportionality must be maintained over a bandwidth sufficient for the measurement. These signals are passed through analog anti-aliasing filters and sampled and digitized by analog-to-digital converters. In the analysis system, blocks of digitized data are Fourier transformed and samples of the needed auto- and cross-power spectral densities are generated by complex-conjugation and multiplication operations. Many successive samples of the spectral densities are averaged to obtain estimates having the needed statistical precision.

2.2 Spectral Densities and Coherence Amplitudes

According to the theory,[2] the expectation values of the spectral densities are as follows:

$$G_{11} = \left| h_1(\omega) \right|^2 F_c \left(31\overline{q_\alpha^2} + \overline{q_c^2} \right), \tag{1}$$

$$G_{22} = \left| h_2(\omega) \right|^2 \left[F W_2 \overline{q_2^2} + \frac{W_2^2 \overline{q_2^2}}{\overline{\nu}^2} \left| H_s(\omega) \right|^2 G_s \right], \tag{2}$$

$$G_{23} = h_2^*(\omega) h_3(\omega) \frac{W_2 W_3 \overline{q_2}\, \overline{q_3}}{\overline{\nu}^2} \left| H_s(\omega) \right|^2 G_s, \tag{3}$$

$$G_{12} = \overline{q}_c h_1^*(\omega) h_2(\omega) \frac{W_2 \overline{q_2}}{\overline{\nu}} H_s(\omega) G_c', \tag{4}$$

where

$h_i(\omega)$ = frequency, ω, response of detection system i,

F_c, F = ^{252}Cf fission rate, reactor fission rate,

q = charge released per interaction in a detector or the ^{252}Cf chamber (subscript α refers to alpha decay and subscript c to spontaneous fission of ^{252}Cf),

W_2, W_3 = detection efficiency in counts per reactor fission for detectors 2 and 3, respectively (W_1 = 1),

$\bar{\nu}$, $\bar{\nu}_i$, $\bar{\nu}_c$ = average number of prompt neutrons per reactor fission, per inherent source fission, per ^{252}Cf fission,

$H_s(\omega)$ = source transfer function of the reactor.

Now, the source spectral density, G_s, is

$$G_s = \bar{\nu}^2 XFR \left[1 + \frac{V}{XR} + \frac{F_i I_i}{FI} \frac{\overline{\nu_i^2}}{XR\bar{\nu}^2} + \frac{F_c}{F} \frac{I_c}{I} \frac{\overline{\nu_c^2}}{XR\bar{\nu}^2} \right] = \bar{\nu}^2 X'FR , \qquad (5)$$

where X is the neutron dispersion number or Diven factor $\overline{\nu(\nu - 1)}/\bar{\nu}^2$; X' is a modified form of the neutron dispersion number defined by Eq. (5); R is the factor which corrects point kinetics for spatial effects;[8-10] I, I_c, and I_i are the importances of neutrons from reactor fission, ^{252}Cf fission, and inherent source fission, respectively; and V equals $(2\beta - \rho)/[(1 - \beta)\bar{\nu}]$, where β is the effective delayed-neutron fraction and ρ is the reactivity. The source spectral density G_s can be expressed as the sum of the three terms G_f, G_i, and G_c indicated in Fig. 1; these represent neutron noise contributions from reactor fission, the inherent source, and ^{252}Cf fissions. Only the neutron noise from ^{252}Cf fission contributes to G_{12} and G_{13}. The correct source term for Eq. (4) is not G_c but G_c', equal to $F_c I_c \overline{\nu_c}/I$. None of the reactors in this study contained an external source, but, if one were present, its parameters could be incorporated by adding another term to G_s similar to that for the inherent source. There are expressions similar to Eqs. (2) and (4) for G_{33} and G_{13} .

The square of the coherence between detectors 1 and 2, i.e., $\gamma_{12}^2 = |G_{12}|^2/G_{11}G_{22}$, can be written as

$$\gamma_{12}^2 = \frac{1}{B_c(1 + C_\alpha)} \left(\frac{\bar{\nu}_c I_c}{\bar{\nu} I}\right)^2 \frac{F_c}{F} \frac{1}{RX'} [1 + 1/Q_2(\omega)]^{-1} , \qquad (6)$$

where

$$Q_2 = \frac{W_2 X' R}{B_2 \Lambda^2} \frac{1}{(\alpha^2 + \omega^2)} , \qquad (7)$$

Λ = prompt-neutron generation time

α = prompt-neutron decay constant

and

$$C_\alpha = 3\overline{1q_\alpha^2} \Big/ \overline{q_c^2} \; ; \quad B_2 = \overline{q_2^2} \Big/ \bar{q}_2^2 \; , \quad B_c = \overline{q_c^2} \Big/ \bar{q}_c^2 . \qquad (8)$$

The square of the coherence between detectors 2 and 3, γ_{23}^2, is $\{[1 + 1/Q_2(\omega)] [1 + 1/Q_3(\omega)]\}^{-1}$, and an expression similar to Eq. (6) gives the coherence between detectors 1 and 3.

Values of the low frequency ($\omega \ll \alpha$) coherence for the ^{252}Cf measurement γ_{12} and the two detector measurements γ_{23} were calculated with parameters typical of an LMFBR (engineering mock-up core for the Fast Flux Test Facility reactor)[11] and typical of the uranium metal assemblies for reactivities from 0.1 to 100 dollars and for detection efficiencies, W, from 10^{-6} to 10^{-1} count per reactor fission ($W_1 = 1$, $W_2 = W_3 = W$). The values of the parameters typical of the Fast Flux Test Facility Reactor were: X = 0.80, R = 1.10, β = 0.0030, $\bar{\nu}$ = 2.91, $\bar{\nu}_c$ = 3.72, C_α = 0.10, $B_c = B_2 = B_3$ = 1.20, I_c/I = 1.15 for a centrally located ^{252}Cf chamber, and $F_c > F_i$. The values of the parameters used in the calculations for the uranium cylinders with no inherent source ($F_i = 0$) were: X = 0.80, R = 1.14, β = 0.0066, $\bar{\nu}$ = 2.60, $\bar{\nu}_c$ = 3.72,

$B_c(1 + C_\alpha) = 1.37$, $B_2 = B_3 = 1.20$, and I_c/I from 0.60 to 0.86 (for a ^{252}Cf chamber on axis adjacent to a flat surface) depending on the reactivity or the uranium cylinder height. The calculated results are plotted in Figs. 2 and 3. With these coherence values, the measurement time can be estimated from the following relation for the relative standard deviation of the power spectral density:[12]

$$c_{ij} \approx \left[\frac{0.5 + \dfrac{1}{\gamma_{ij}^2}}{2\Delta f T} \right]^{1/2} , \qquad (9)$$

where Δf is the bandwidth of the analyzer, and T is the total sampling time. In a digital Fourier analyzer, $\Delta f T$ is the total number of samples. For a near-critical or a slightly subcritical reactor, the coherence γ_{12} for the ^{252}Cf measurement is less than the coherence γ_{23} for the two-detector noise measurement; thus the measurement with ^{252}Cf will require more time to achieve the same precision in the CPSD. With a reactor at far subcritical, a measurement with ^{252}Cf will take less time. Near criticality, where $[1 + 1/Q_2]^{-1}$ is at its maximum, the coherence γ_{12}^2 is low because of the relatively small value of F_c/F, which results from the relatively high multiplication of the reactor. As the reactivity is reduced, the decrease in $[1 + 1/Q_2]^{-1}$ tends to be compensated by the increase in F_c/F. Thus, the coherence for the ^{252}Cf measurement does not vary with reactivity as much as the coherence for the two-detector noise measurement. This means that a measurement of G_{12} with detection efficiency $<10^{-4}$ will take the same time slightly subcritical (0.1 dollar) as it will far subcritical ($>\sim 30$ dollars). Although it is advantageous for reactors with inherent sources to have the ^{252}Cf source stronger than the inherent source, further increases in the size of the ^{252}Cf source are not beneficial because there is no further improvement in the ratio F_c/F, since F also includes fissions from fission chains initiated by neutrons from ^{252}Cf. The estimated measurement times to achieve a given precision for the ^{252}Cf measurement, obtained from these values of the coherence (γ_{12}), are somewhat longer than those given by Seifritz.[13]
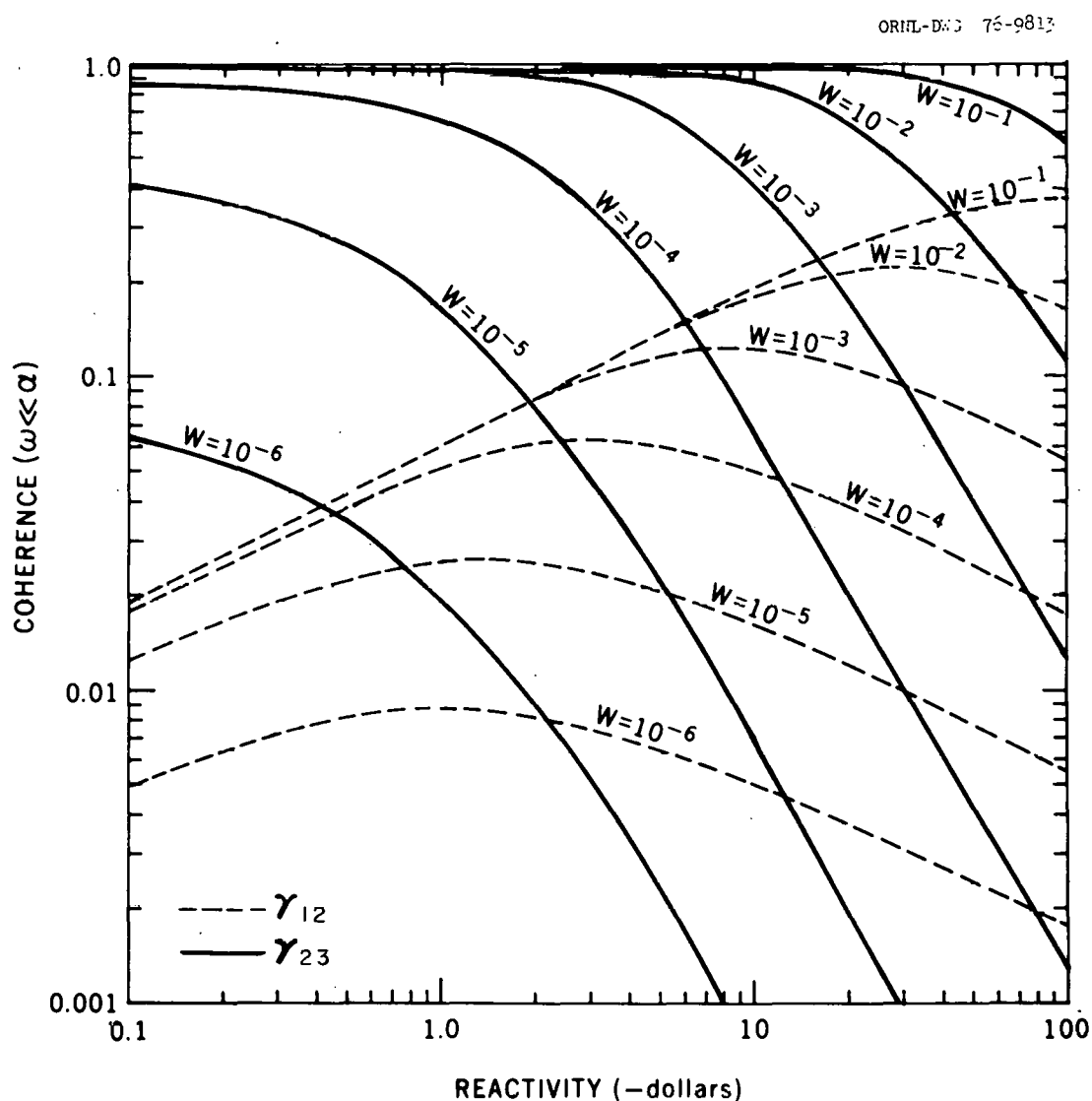
Fig. 2. Coherence amplitudes ($\omega \ll \alpha$) as a function of subcritical reactivity for various detection efficiencies for the FFTF.

ORNL-DWG 76-9814
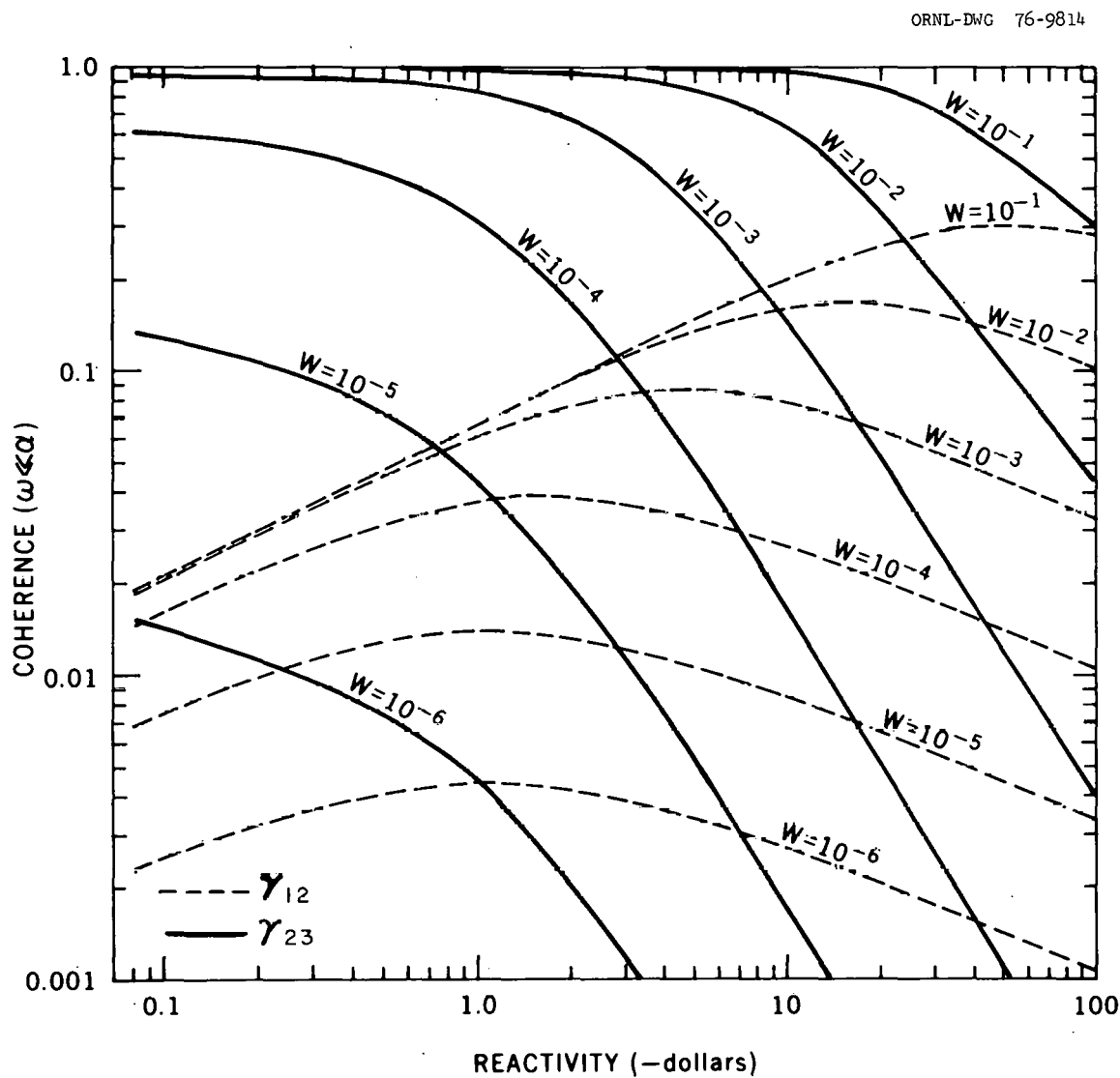
Fig. 3. Coherence amplitudes ($\omega \ll \alpha$) as a function of subcritical reactivity for various detection efficiencies for uranium metal cylinders.

The coherence values show that for detection efficiency values of 10^{-6}, 10^{-5}, 10^{-4}, 10^{-3}, and 10^{-2} the precision of G_{12} will be better than that for G_{23} if the subcritical reactivities are larger than 2, 5, 13, 30, and 70 dollars, respectively, for measurements made with the FFTF reactor. Similar reactivity values for the uranium cylinder measurements were a factor of ~ 2 smaller.

2.3 Reactivity Determinations

The methods for determination of the reactivity from the power spectral densities given by Eqs. (1) to (4) can be classified into three categories: (1) the existing methods related to the conventional two-detector auto- and cross-power spectral densities, G_{22}, G_{33}, and G_{23}; (2) those that determine parameters which have been used previously for reactivity determinations from the cross-power spectral densities with ^{252}Cf, G_{12}; and (3) new methods that determine the reactivity without a calibration near delayed criticality.

The use of previously described neutron noise methods,[14-18] such as the determination of the reactivity from the breakfrequency of auto-power spectral densities (APSDs) and CPSDs or from the coherence amplitude, γ_{23}, requires a knowledge of the breakfrequency and coherence amplitude at some reference state, usually near delayed criticality, for which the reactivity is known, as well as the change in the prompt-neutron generation time or detection efficiency between the reference state and the reactivity state of interest. These breakfrequency noise analysis[14-18] methods require corrections for the frequency response functions of the detection system, $h_2(\omega)$ and $h_3(\omega)$, which are usually obtained from measurements in which the detection system is exposed to the random emission of a neutron source [this input is a white noise source, and, thus, the measured frequency response will be $h_i(\omega)$]. The modified source multiplication method also requires correction for changes in detection efficiency and source intensity.[19,20] These methods of reactivity determination are difficult to apply in the initial startup of a reactor because they require a calibration near delayed criticality.

The measurement of the cross-power spectral density with ^{252}Cf allows the determination of the breakfrequency, from which the prompt-neutron decay constant can be obtained. After a correction is made for the frequency response of the detection systems, the CPSD, G_{12}, is proportional to the source transfer function of the reactor $[(\alpha + i\omega)\Lambda]^{-1}$, and $|G_{12}|^2$ can be fitted by a least-squares method to determine the value of α. This measurement also allows the determination of the prompt-neutron decay constant in another way, since the source transfer function can be written as $(\alpha - i\omega)/(\alpha^2 + \omega^2)\Lambda$, and thus G_{12} has a real and an imaginary part which can be obtained by present digital Fourier analyzers. Since the values of ω are known, the product of the ratio of the real to the imaginary part of G_{12} and the frequency ω is constant and equal to the prompt-neutron decay constant. In principle, a high precision measurement at one frequency should yield the prompt-neutron decay constant. The subcritical reactivity can be obtained from the ratio of this decay constant to that for the calibration state after it has been corrected for the change in the neutron lifetime from the calibration state to the subcritical state of interest. In practice, this product would be obtained over a wide range of frequencies. The constancy of this product can be used to validate the point kinetics model since the presence of higher modes would cause the value of α determined in this way to be a function of frequency. The constancy of the ratio would also verify whether the correction for the frequency response of the instrumentation is correct.

Various combinations of spectral densities were examined in order to determine if any additional information could be obtained from the simultaneous measurement of all four spectral densities represented by Eqs. (1), (3), and (4) with its analogue. To develop a method for measuring the reactivity, consider the following combination of spectral densities:

$$\frac{G_{12}^{*}G_{13}}{G_{11}G_{23}} = \frac{\gamma_{12}\gamma_{13}}{\gamma_{23}} = \frac{1}{B_c(1 + C_\alpha)}\left(\frac{\bar{\nu}_c I_c}{\bar{\nu} I}\right)^2 \frac{1}{RX'}\frac{F_c}{F} \quad . \tag{10}$$

The ratio of spectral densities given in Eq. (10) is independent of frequency. Thus, the constancy of Eq. (10) as a function of frequency could be used to validate the model as well as to determine whether the experimental data from the noise analysis measurement have adequate precision. Since $F\bar{I\nu} = (F_c I_c \bar{\nu}_c + F_i I_i \bar{\nu}_i) \frac{k}{1-k}$, Eq. (10) can be rearranged to yield the subcritical reactivity ρ in Δk units, where k is the neutron multiplication factor, including the effect of delayed neutrons. Thus,

$$\frac{1-k}{k} = \frac{G_{12}^* G_{13}}{G_{11} G_{23}} \frac{(F_c I_c \bar{\nu}_c + F_i I_i \bar{\nu}_i)}{(F_c I_c \bar{\nu}_c)} \frac{I\bar{\nu}}{I_c \bar{\nu}_c} B_c (1 + C_\alpha) X'R \ . \tag{11}$$

No correction for the frequency response of the instrumentation is required, because the transfer functions for the detection system electronics are cancelled in forming the ratio given by Eq. (10). Since X' defined by Eq. (5) contains the reactivity and differs from X far subcritical, Eq. (11) should not be used for far subcritical reactivities. Substitution for X' and rearrangement gives the following more accurate expression for the subcritical reactivity $[-\rho = (1-k)/k]$:

$$-\rho = \frac{G_{12}^* G_{13}}{G_{11} G_{23}} \frac{YP_1 P_4}{1 - \frac{G_{12}^* G_{13}}{G_{11} G_{23}} \frac{YP_1 P_5}{\beta}} = (L_4 Y) \frac{P_1 P_4}{1 - L_4 Y \frac{P_1 P_5}{\beta}} \ , \tag{12}$$

where

$$L_4 = G_{12}^* G_{13} / G_{11} G_{23} \ ,$$

$$Y = (F_c I_c \bar{\nu}_c + F_i I_i \bar{\nu}_i)/F_c I_c \bar{\nu}_c \ , \tag{13}$$

$$P_1 = B_c (1 + C_\alpha) RXI\bar{\nu}/I_c \bar{\nu}_c \ , \tag{14}$$

$$P_2 = \left[\frac{\bar{\nu}_i^2}{\bar{\nu}_i} (Y - 1) + \frac{\bar{\nu}_c^2}{\bar{\nu}_c} \right] \Big/ XRY \ , \tag{15}$$

$$P_3 = 2\beta/XR(1 - \beta)\bar{\nu} \,, \tag{16}$$

$$P_4 = 1 + P_3 \,, \tag{17}$$

$$P_5 = \frac{P_3}{2} + \frac{\beta P_2}{\bar{\nu}} \,. \tag{18}$$

Equations (11) and (12) do not depend on detection efficiency, but do depend on the properties of the counter containing ^{252}Cf, $B_c(1 + C_\alpha)$, which can be determined outside the reactor. The ratio of the effective neutron production rates, Y, can be determined from the change in count rate when the ^{252}Cf source is inserted into the subcritical reactor. The values of R and X can be determined from calculation and other measurements and are insensitive to large changes in reactivity. The values of the numbers of neutrons per fission are known, and the relative importance I/I_c can be calculated or obtained from other measurements. Thus, Eq. (12) gives the reactivity or neutron multiplication factor in k units. This method requires neither a calibration near delayed criticality nor corrections for neutron lifetime and detection efficiency changes, which the other noise analysis methods require.

For a pulse mode electronics system and a ^{252}Cf chamber in which all the alpha pulses can be discriminated, $C_\alpha = 0$, $B_c = 1$, and Eq. (10) reduces to $\left(\dfrac{\bar{\nu}_c I_c}{\bar{\nu} I}\right)^2 \dfrac{1}{RX} \dfrac{F_c}{F}$. Thus, for pulse mode operation of the ^{252}Cf ionization chamber, the reactivity does not depend on the properties of the californium fission detection system.

The reactivity can be determined in another way by considering the ratio of the real part of G_{12} to the magnitude of G_{23} . The CPSDs G_{12} and G_{23} require correction for the frequency response of the instrumentation, which is measured in a calibration assembly consisting of the ^{252}Cf source and the two detectors (detectors adjacent with the source between them and all isolated from the reactor or significant amounts of moderator that could introduce a frequency dependence other than that

of the detection system electronics). The corrected spectral density,[a] G'_{c12}, is

$$G'_{c12} = \frac{G_{12}}{G_{A12}} = \frac{\bar{\nu}_c F_c I_c J_2 H_s(\omega)}{\bar{\nu} F I J_{A2}} , \qquad (19)$$

where subscript A denotes a spectral density measured with the calibration assembly, and J_2 and J_{A2} are the current from detection system 2 in the reactor measurement and the calibration measurement, respectively.

The CPSD G_{23} may be corrected for the frequency response of the instrumentation by using APSDs, and its squared magnitude is

$$|G_{c23}|^2 = \frac{G_{23}^* G_{23}}{G_{A22} G_{A33}} = \left(\frac{J_2 J_3}{F} RX'\right)^2 \frac{\bar{q}_{A2}}{J_{A2} J_{A3} \bar{q}_{A2}^2} \frac{\bar{q}_{A3}}{\bar{q}_{A3}^2} |H_s(\omega)|^4 . \qquad (20)$$

The ratio of the real part of G'_{c12} to the magnitude of G_{c23} is independent of frequency and is given by

$$\frac{Re(G'_{c12})}{G_{c23}} = \left(\frac{1 - k_p}{k_p}\right) \frac{I_c \bar{\nu}_c}{I \bar{\nu}} \left[\frac{J_{A3}}{J_{A2}} \frac{\bar{q}_{A2}^2 \bar{q}_{A3}^2}{\bar{q}_{A2} \bar{q}_{A3}}\right]^{1/2} \cdot \frac{1}{RX'} \frac{F_c}{\bar{q}_3 F W_3} , \qquad (21)$$

where k_p is the prompt neutron multiplication factor and $\alpha\Lambda = (1 - k_p)/k_p$.

To obtain the ratio [Eq. (21)] with better precision, the integrals of G_{12} and G_{23} over frequency can be used. This ratio can be large for a low detection efficiency. The unknown quantities in Eq. (21) are the

---

[a]The correction to a CPSD G_{23} for the frequency response of the instrumentation may be made by dividing by the square root of the product of auto-power spectral densities (G_{A22} and G_{A33}) or by the cross-power spectral density (G_{A23}) obtained with the source and detectors adjacent and isolated. However, it is usually more accurate to make the correction in the conventional way using APSDs as indicated in Eq. (20). Prime notation on spectral density indicates correction by a CPSD from a calibration measurement, as in Eq. (19).

current (q_3FW_3) and the currents and the charges in the calibration meas-urement, which can be measured. The other quantities on the right side of Eq. (21) are known constants, except for the spatial-effects factor R and the ratio of the importance of the neutrons from ^{252}Cf fission to those from reactor fission, and they are obtained as described previously. This expression for pulse mode operation of all detection systems corresponds to an expression that has previously been employed in time domain meas-urements (refs. 1, 21-23). An alternative form of Eq. (21) that is sometimes convenient for calculations is

$$\text{Re} G'_{c12}/G_{c23} = \left(\frac{1 - k_p}{k_p}\right) \frac{I_c \bar{v}_c}{I\bar{v}} \frac{1}{RX'} \frac{1}{B_c(1 + C_\alpha)} \frac{1}{\gamma_{A12}\gamma_{A13}} \frac{J_{A3}}{J_3} . \qquad (22)$$

An alternative method of combining G_{12} and G_{23} while eliminating the frequency response of the instrumentation is given in Eq. (23):

$$\text{Re}\left(\frac{G^*_{12}G_{A13}}{G_{23}G_{A11}}\right) = \left(\frac{1 - k_p}{k_p}\right) \frac{I_c \bar{v}_c}{I\bar{v}} \frac{1}{RX'} \frac{1}{B_c(1 + C_\alpha)} \frac{J_{A3}}{J_3} . \qquad (23)$$

A similar expression for $\text{Re} \, G^*_{A12}G_{13}/G_{A11}G_{23}$ is obtained by replacing J_{A3}/J_3 with J_{A2}/J_2, and J_i (i = 2,3) = $F\bar{q}_i W_i$. Equations (22) and (23) are related as follows:

$$\text{Re}\left(G^*_{12}G_{A13}/G_{23}G_{A11}\right) = \gamma_{A12}\gamma_{A13} \, \text{Re}\left(G_{c12}/G_{c23}\right) . \qquad (24)$$

The new methods of reactivity determination proposed enable the determination of subcriticality without a knowledge of the properties of the reactor or critical assembly at delayed criticality. The fre-quency domain measurements which use Eq. (21), the ratio of the real part of the CPSD with ^{252}Cf to the absolute value of the CPSD between the pair of neutron detectors, require a calibration measurement with a white noise source to eliminate the frequency response functions

for the instrumentation system. These response functions could be meas-
ured outside the reactor before the instrumentation is installed in the
reactor; but once installed, the response functions must not change.

The difficulty of the preceding method [Eqs. (21)-(23)] caused by
the requirement of measurement of the frequency response functions for
the instrumentation systems can be avoided by using the other frequency
domain method [Eq. (12)] that measures the ratio $G_{12}^{*}G_{13}/G_{11}G_{23}$. The
ratio is frequency independent, and the required properties of the
^{252}Cf chamber can be determined outside the reactor. This method also
requires the ratio of the neutron production rates with and without
the californium source in the reactor [Eq. (13)]. This ratio can be
determined from the ratio of count rates from the source range monitor-
ing system for the reactor with and without the ^{252}Cf source in the
reactor. The ratio of importance-weighted neutron production rates is
usually not sensitive to fuel loading or detector location for a cen-
trally located ^{252}Cf source (see Table 2, p. 33).

These methods assume that the application of the point kinetics
equations to the subcritical state of interest is valid. However, they
do provide verification of this assumption in each measurement. If more
than one decay mode is significant, the ratio of the real to the imagi-
nary part of G_{12} multiplied by the frequency will not be constant with
frequency. Since these methods do not require calibration at a known
reactivity state, they can be used in the initial loading of a reactor
where subcriticality determinations cannot depend on some calibration
near delayed criticality. Also, the interpretation of the measured data
to obtain the reactivity does not depend on the relative or absolute
values of the source intensity or detection efficiency. These methods
may also be useful in determining the reactivity of assemblies where
loading to criticality is undesirable or where sufficient fissionable
material to achieve criticality is not available. These methods do
require a detector with high efficiency.

3. EXPERIMENTS WITH THE ENGINEERING MOCK-UP CORE FOR FFTF

To test this method for possible application in initial loading of
LMFBRs, these types of measurements were added to experiments at Argonne
National Laboratory (ANL) simulating the initial loading of the engineer-
ing mock-up core for the FFTF. Since these were add-on experiments to
an existing experimental sequence, a maximum of only 12 days was allotted
for these measurements.

3.1 Description of the Mock-up Core

The engineering mock-up core for the FTR at the ZPR-9 facility of
ANL has previously been described.[24,25] The locations of the detectors
for the power spectral density measurements are shown in a sketch of the
loading of the mock-up core for the reverse approach to critical experi-
ment (Fig. 4). A 15-μg ^{252}Cf source was placed at the approximate center
of the core (10 cm back from the midplane on the fixed half of the
assembly) in one of the four assembly drawers mocking up a material test
loop (MT 203) in the second row of fuel assemblies from the core center
(in the ZPR-9 assembly, FTR components are mocked up by 2 × 2 drawer
assemblies). A pair of fission counters was installed initially in the
mock-up of the same loop (10 cm back from the midplane on the movable
half of the assembly) and a pair of ^{6}Li-glass scintillators was installed
in two of the four drawers mocking up a general purpose test loop
(GP 403) in the fourth row of fuel assemblies from the center of the
inner core. After the initial measurements, the locations of the pairs
of detectors were interchanged.

Measurements were performed for six different configurations[a] with
reactivities down to ∿75 dollars subcritical where the reactivity was
changed by removal of fuel or neutron absorbing material. These configu-
rations in which the inner core was fully loaded were: (1) all fuel in
rows 5 and 6 of the outer core with all FTR safety and control rods

---

[a]Rows 5 and 6 are the inner and outer fuel rows, respectively, of
the outer core zone of the FFTF.

ORNL-DWG 74-10770R

TRISECTOR 2   LLFM SHIELD

Sodium Ring

RADIAL REFLECTOR

F

PSR 714

OUTER CORE

CR 508

CR 506

SR 304

L
L

F
C F

CR 514

SR 308

F

SR 312

INNER CORE

CR 516

PSR 702

CR 524

CR 522

PSR 726

Shield

F

LLFM

Shield

F

LLFM

TRISECTOR 1

SR	SAFETY ROD
CR	CONTROL ROD
PSR	PERIPHERAL SHIM ROD

TRISECTOR 3

F   FISSION COUNTER

L   LITHIUM DETECTOR

C   CALIFORNIUM CHAMBER
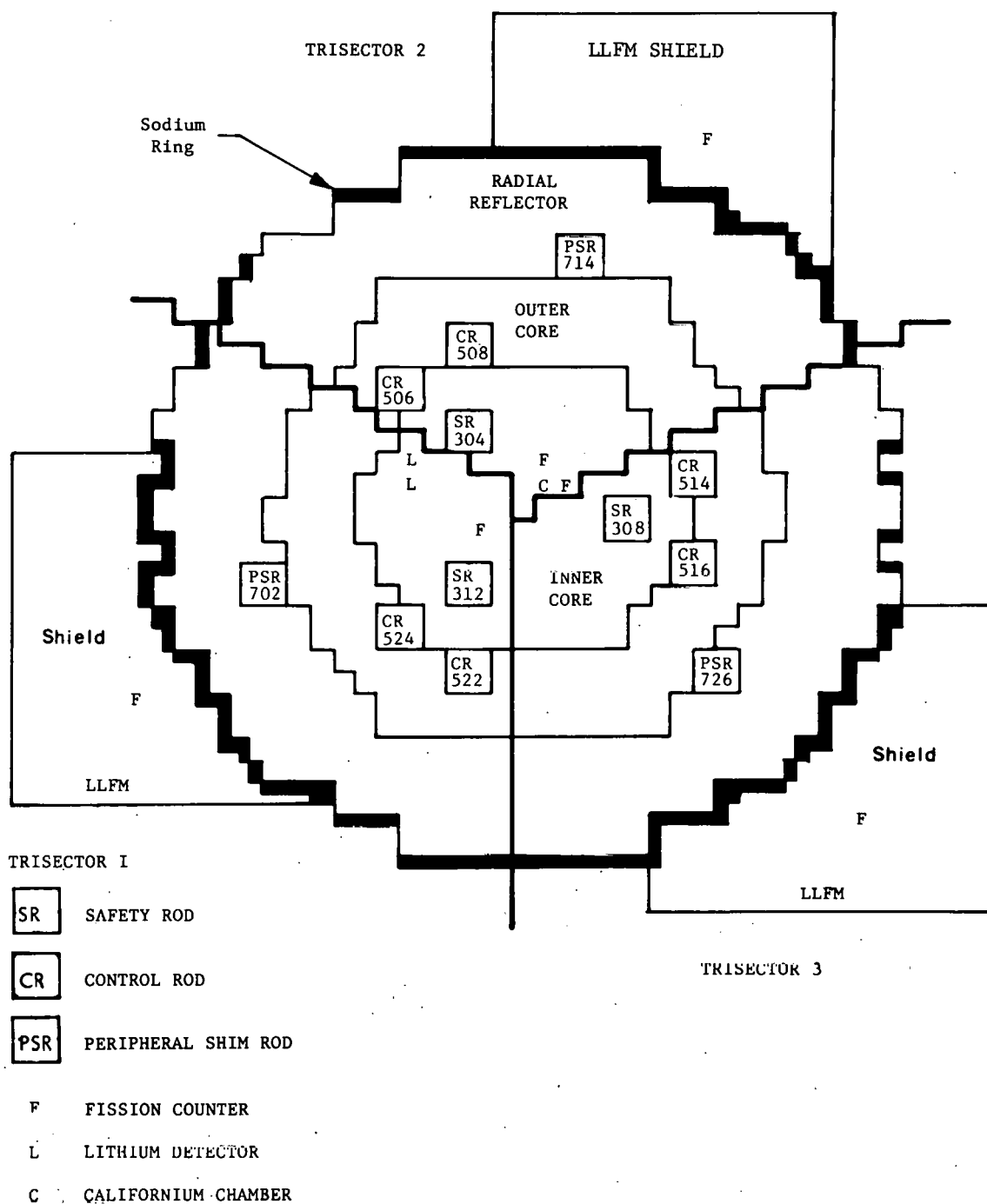
Fig. 4. Sketch of the loading of the engineering mock-up core for the FFTF on the stationary half of the ZPR-9 facility, at the midplane. (LLFM signifies the low level flux monitor fission counter in the shield.)

withdrawn except control rod 514 of trisector 3 (TS-3); (2) also with all safety and control rods inserted; (3) three fuel subassemblies removed from row 6 of TS-3 with all safety and control rods withdrawn except safety rod 308 and control rods 524, 514, and 516 for two configurations of detectors; (4) all fuel removed from row 6 of TS-3 with all safety and control rods inserted; (5) all fuel removed from rows 5 and 6 of TS-3 with allsafety and control rods withdrawn except those of TS-3, and with the ^{252}Cf source 10 and 30 cm from the midplane; and (6) fuel of rows 5 and 6 removed from TS-2 and TS-3 with all safety and control rods inserted.

3.2 Detectors and Instrumentation

Except for the ^{252}Cf chamber, the instrumentation systems used in the spectral density measurements with ^{252}Cf were similar to those described previously.[26-28] The location of the preamplifiers in the assembly adjacent to the Li-glass scintillators (3.8 cm diam and 2.5 cm thick, with 6.6 wt % Li enriched to 95% in ^{6}Li) extended the flatness of the frequency response to 68 kHz. The intensity of the ^{252}Cf source was chosen so that the fission rate of the engineering mock-up core would double when the source was placed in the center. The auto-power spectral density from the ^{252}Cf ionization chamber system operating in both the current and pulse mode shortly after assembly is shown in Fig. 5 for frequencies up to 100 kHz. The rolloff at 70 kHz results from the cutoff of the anti-aliasing filter, which in these measurements was ∿70% of the maximum frequency for all detection systems. The rolloff at low frequency in the current mode operation results from the ion mobility in the ^{252}Cf chamber. For a chamber with stationary characteristics, this power spectral density is fixed since it depends only on the chamber characteristics and not the reactor properties. The properties of the chamber used for these measurements were not stationary, and the changing spectral densities precluded reactivity determination by these methods. These changes were accompanied by the inability in pulse mode operation to discriminate alpha particle decay from spontaneous fission a few weeks after initial fabrication, and thus, made measurements in the pulse mode of the engineering mock-up core impractical. The schedule of the measurements
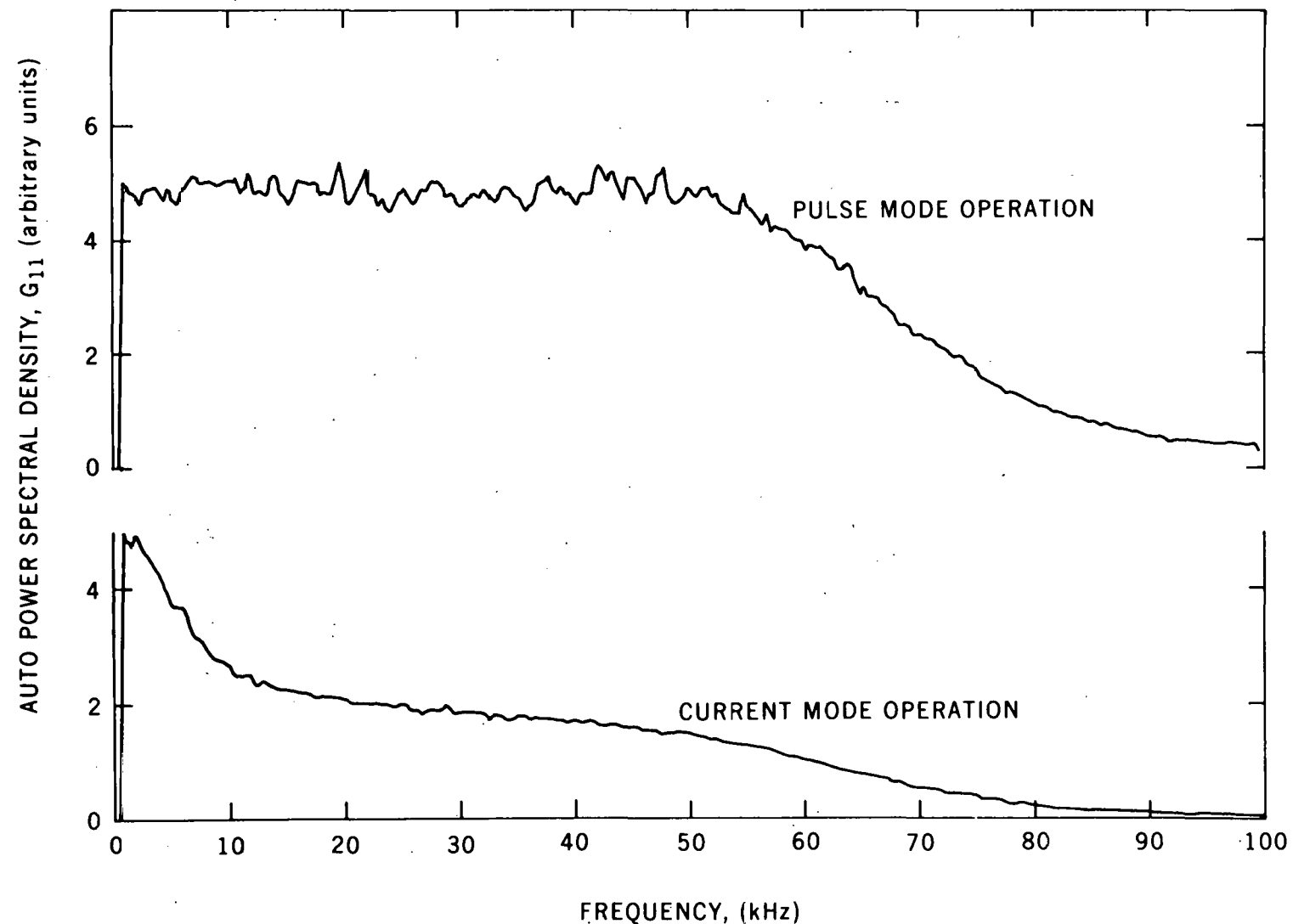
Fig. 5. Power spectral densities for the ^{252}Cf (15 μg) chamber in pulse and current mode operation (pulse mode data were taken just after initial assembly of chamber).

precluded chamber refabrication. The deterioration of the chamber was not corrected by subsequent gas refilling at ANL with $Ar-CO_2$ instead of CH_4.

3.3 Power Spectral Densities

Three input channels of the four-channel, 200-kHz, 12-bit ADC were used (one for the ^{252}Cf chamber and the others for the two detectors). The software for the noise analyzer[29] was modified so that the following data for 256 frequency points were collected in the measurement: (1) the auto-power spectral densities of the ^{252}Cf chamber and a pair of detectors, G_{11}, G_{22}, and G_{33}; (2) both the real and the imaginary parts of the cross-power spectral densities between the detectors and between each detector of a pair and the ^{252}Cf chamber, G_{23}, G_{12}, and G_{13}; and (3) the standard deviations of G_{23} and of the real part and the imaginary part of G_{12}. The measurement time required, which included both data sampling and minimal processing, was as large as 270 min for some configurations, but only a small percentage ($\sim2\%$) of this time was for sampling the signals. (The processing time will decrease considerably when faster Fourier transform processors are available.) At the termination of a measurement, these spectra were then used to calculate the coherences, γ_{12}, γ_{13}, and γ_{23}, and the ratio of spectral densities, $G_{12}^{*}G_{13}/G_{11}G_{23}$, for all frequency points. With this software, the spectral densities or a combination of them could be fitted to the appropriate equations to determine the average values of ratios or the breakfrequencies.

Typical power spectral densities for configuration 5 with a reactivity of ~13 dollars subcritical are presented in Figs. 6 to 8. The auto-power spectral density, corrected for the frequency response characteristics of the electronics and anti-aliasing filter, for one of the ^6Li-glass scintillators (Fig. 6) contains the rolloff due to the characteristics of the reactor, and the breakfrequency determined by least-squares fitting of this data is 7840 ± 240 Hz.[a] The corrected cross-power

---

[a]Before fitting to obtain the breakfrequency, the 256 data points were regrouped to 64 as previously described (ref. 29).

ORNL-DWG 75-12760R1
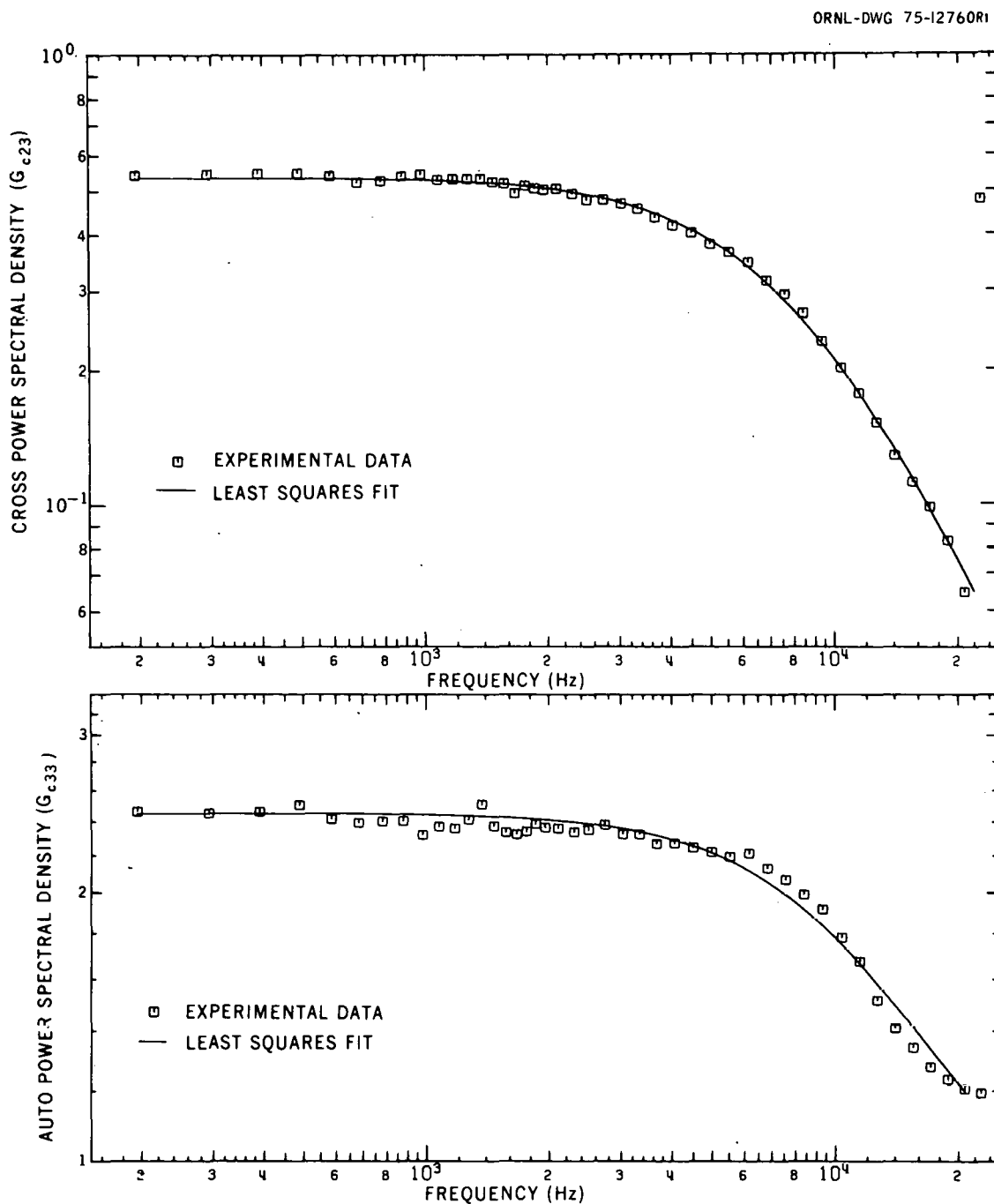
Fig. 6. Cross- (G_{c23}) and auto- (G_{c33}) power spectral densities for the engineering mock-up core for FFTF with all fuel removed from row 5 and 6 of trisector 3 and only control and safety rods of tri-sector 3 inserted (configuration 5).
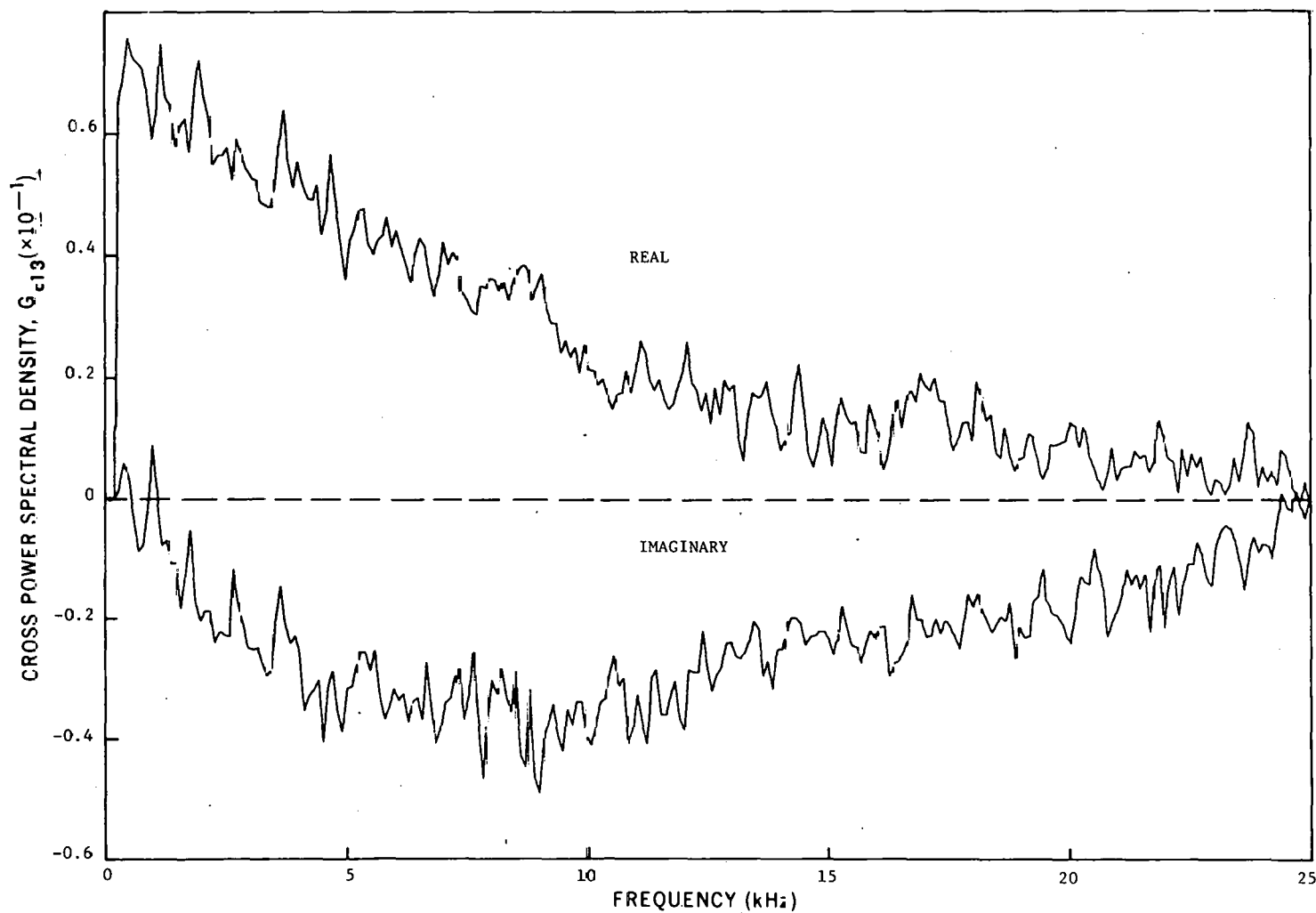
Fig. 7. Real and imaginary parts of the cross-power spectral density with ^{252}Cf for the engineering mock-up core for FFTF with all fuel removed from rows 5 and 6 of trisector 3 and only control and safety rods of trisector 3 inserted (configuration 5).
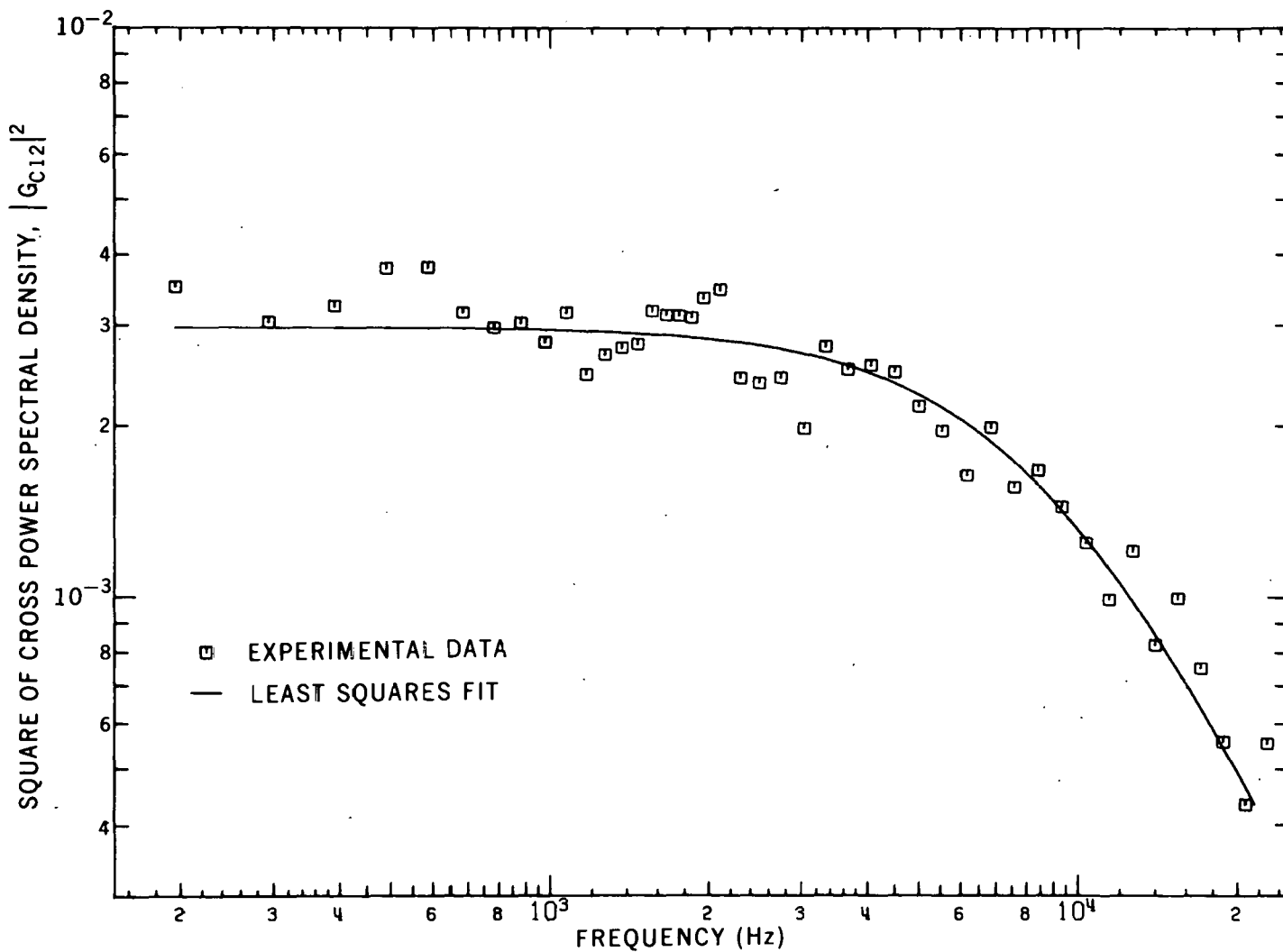
Fig. 8. Square of the cross-power spectral density with ^{252}Cf for the engineering mock-up core for FFTF with all fuel removed from rows 5 and 6 of trisector 3 and only control and safety rods of trisector 3 inserted (configuration 5).

spectral density between the two scintillators is also shown in Fig. 6, and the breakfrequency obtained from a fit of these data is 8020 ± 350. The corrected cross-power spectral density (both the real and imaginary parts) between one of the scintillators and the ^{252}Cf chamber is shown in Fig. 7. The negative values of the imaginary part of G_{c12} are consistent with the theoretical prediction that G_{c12} is proportional to the source transfer function of the reactor. The square of this cross-power spectral density (Fig. 8) was fitted to obtain a breakfrequency of 8150 ± 360 Hz, while the breakfrequency from the square of the cross-power spectral density for the other scintillator with ^{252}Cf was 8930 ± 230 Hz.

3.4 Prompt-Neutron Decay Constant

The ratio of the real to the imaginary part of the corrected cross-power spectral density between one of the scintillators and the ^{252}Cf chamber (Fig. 9) multiplied by the frequency is constant with frequency and has a value of 59,700 ± 1480 sec^{-1}. The erratic large magnitude values at very low and high frequency result from the near-zero values of parts of G_{c13} (Fig. 7). This value of the prompt-neutron decay constant together with that previously measured at delayed criticality can be used to obtain an estimate of the reactivity for this configuration of 12.6 dollars subcritical (neglects small changes in the prompt-neutron lifetime), which agrees with the value of 13.1 dollars obtained from the modified source multiplication measurement.[30] The constancy of this ratio with frequency verifies one of the predictions of the theory and the validity of the point kinetics assumption since nonconstant values would have implied that fundamental mode decay did not exist.

3.5 Coherence Amplitudes

The spectral densities were combined to form the coherence function. Typical plots of both types of coherence as a function of frequency for one of the configurations of the mock-up core are shown in Fig. 10. The values at low frequency obtained in these measurements were $\gamma_{12} = 0.0344 \pm 0.0040$, $\gamma_{13} = 0.0336 \pm 0.0050$, and $\gamma_{23} = 0.214 \pm 0.010$. The coherence,
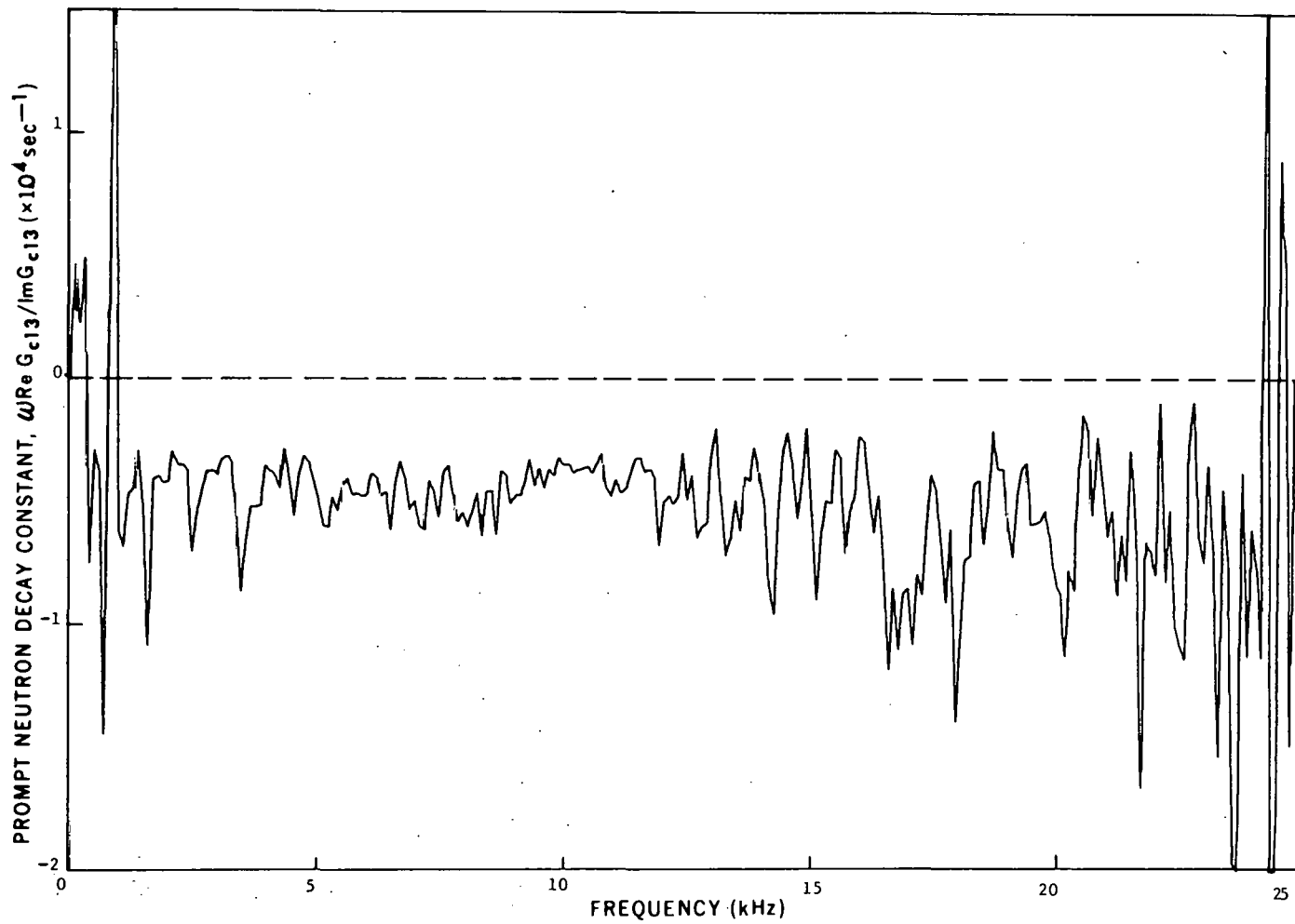
Fig. 9. Prompt-neutron decay constant for the engineering mock-up core for FFTF with all fuel removed from rows 5 and 6 of trisector 3 and only control and safety rods of trisector 3 inserted (configuration 5).
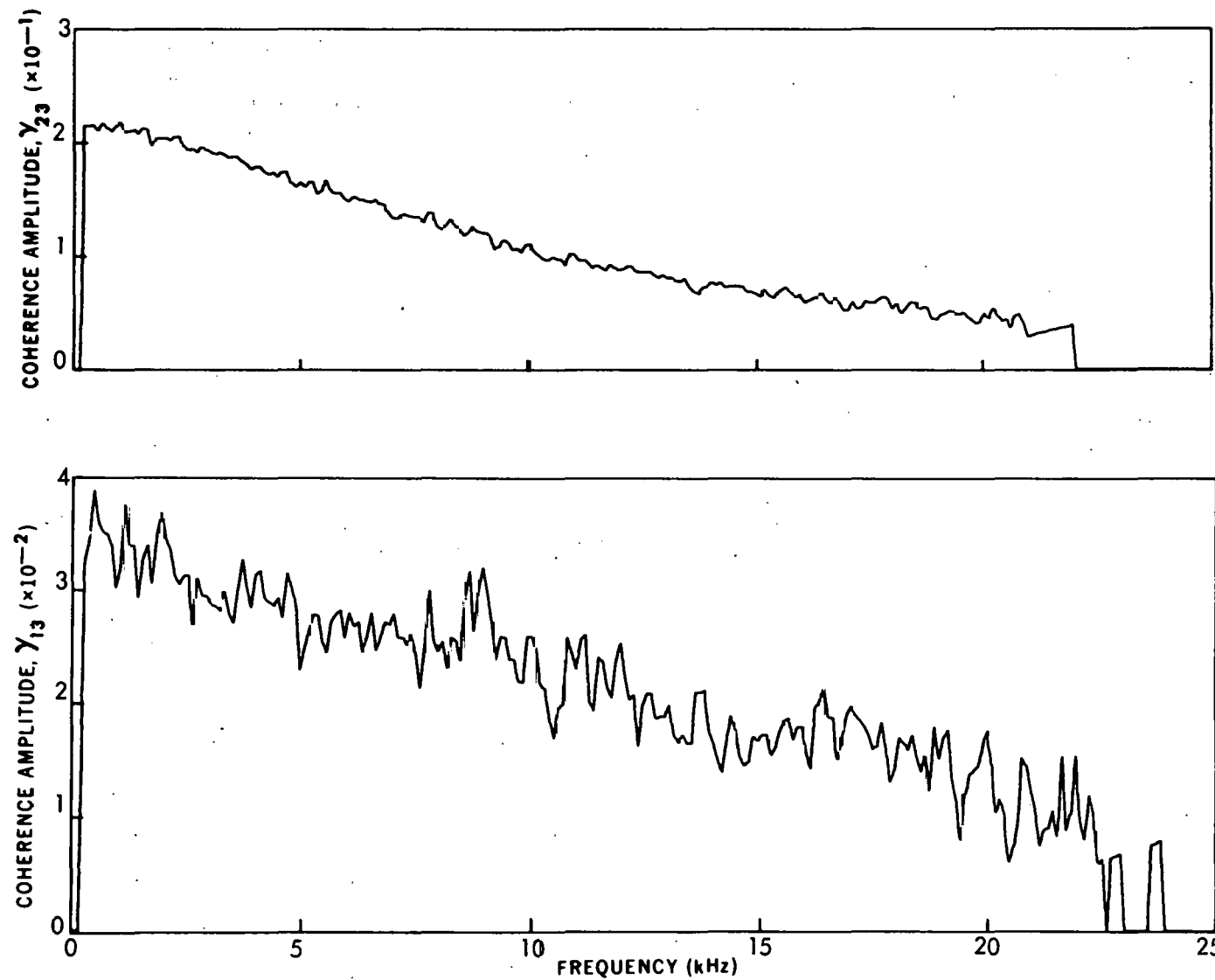
Fig. 10. Coherence amplitudes for the engineering mock-up core for FFTF with all fuel removed from rows 5 and 6 of trisector 3 and only control safety rods of trisector 3 inserted (configuration 5).

γ_{23}, is larger because at this reactivity the fission rate in the assembly, which is the equivalent noise source for the cross correlation between the two scintillators, is much larger than the ^{252}Cf fission rate, which is the equivalent noise source for the cross correlation with ^{252}Cf. Thus, at this reactivity the precision in the spectral densities is larger for the cross correlation between scintillators than between the scintillator and the ^{252}Cf chamber. The values of the coherence at low frequency are plotted in Fig. 11 as a function of the reactivity obtained from modified source multiplication measurements previously reported.[30] The small variation of γ_{13} with reactivity compared to that for γ_{23} confirms the prediction of the theory (Fig. 2) that a measurement which correlates with ^{252}Cf can be done far subcritical in the same time for a given precision as at reactivities near delayed criticality. From these data the cross-power spectral densities with ^{252}Cf can be measured with greater precision for reactivities further subcritical than 50 dollars, and the measurement time to determine the reactivity by Eq. (12) is determined by the precision of the cross-power spectral density measurement between the two scintillators; for reactivities less subcritical than 50 dollars, the time required for a given precision is determined by the cross-power spectral density measurement with ^{252}Cf. For these measurements the structure of software permitted the choice of the number of samples of data for each spectral density determination consistent with the desired precision.

3.6 Ratios of Spectral Densities

Another prediction of the theory is that the ratio of the real part of G_{13} to G_{23}, when corrected for the frequency response of the instrumentation, is a constant. Figure 12 verifies this prediction of the theory. The ratio of spectral densities $G_{12}^{*}G_{13}/G_{11}G_{23}$ is plotted in Fig. 13 as a function of frequency and is also constant up to 15 kHz as predicted by the theory. Beyond 15 kHz the magnitude of the spectral densities is low due to the upper cutoff on the anti-aliasing filter, and the precision of the ratio is very poor.
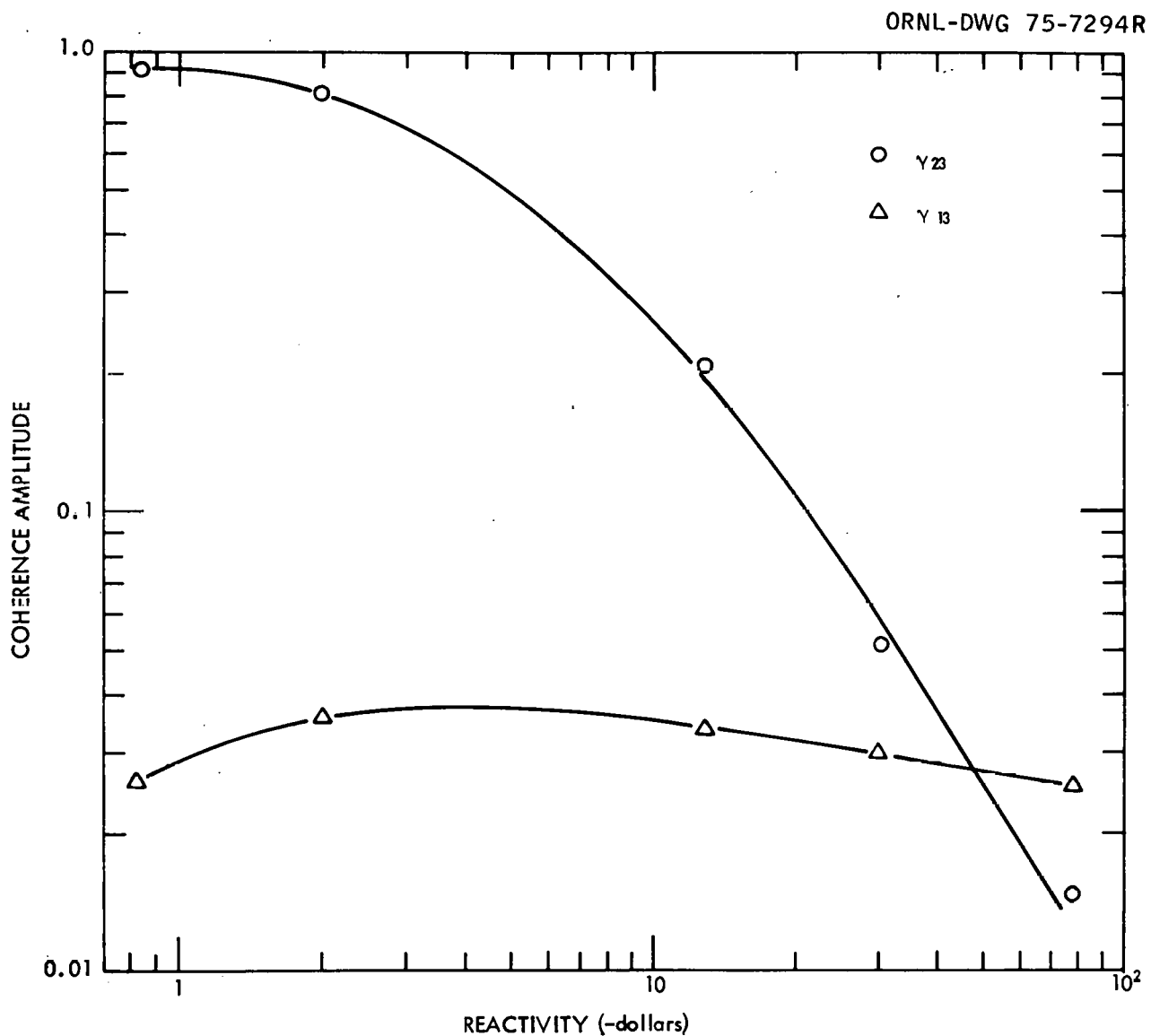
ORNL-DWG 75-7294R

Fig. 11. Coherence amplitude at low frequency as a function of reactivity for initial loading configurations of the engineering mock-up core for the FFTF.
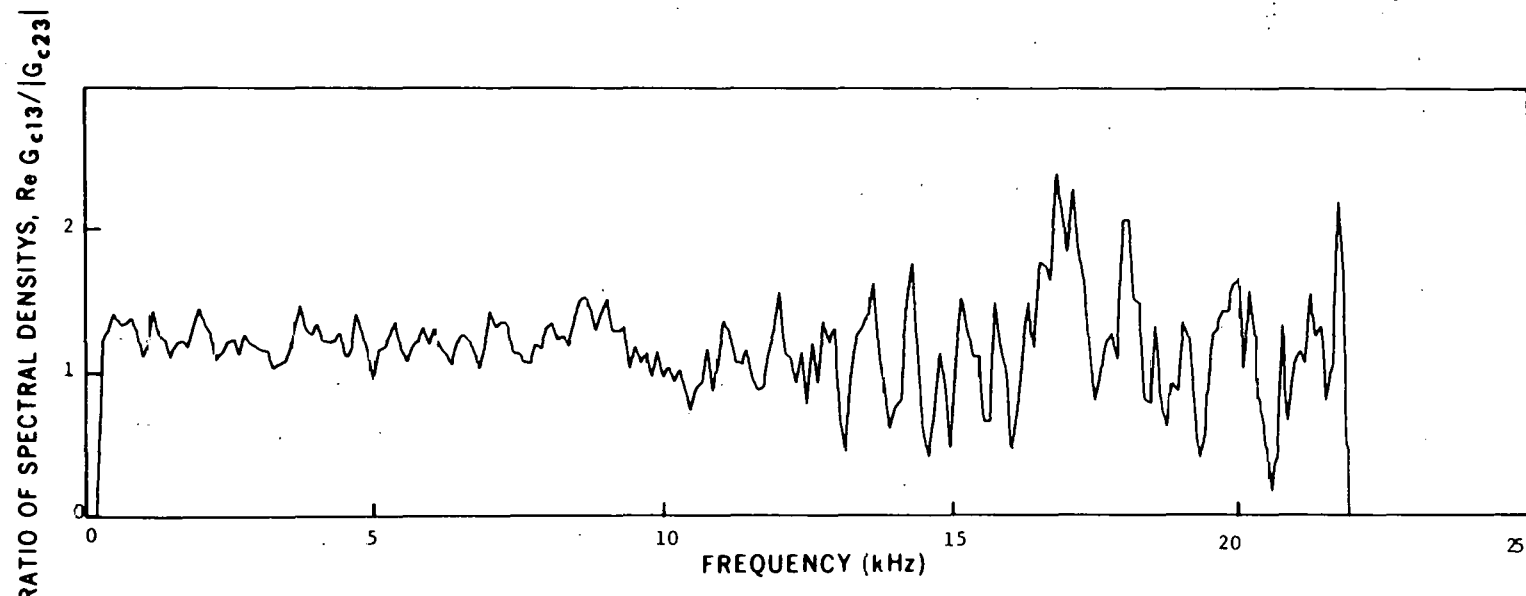
Fig. 12. Ratio of spectral densities ReG_{c13}/G_{c23} as a function of frequency for the engineering mock-up core for FFTF with all fuel removed from rows 5 and 6 of trisector 3 and only control and safety rods of trisector 3 inserted (configuration 5).
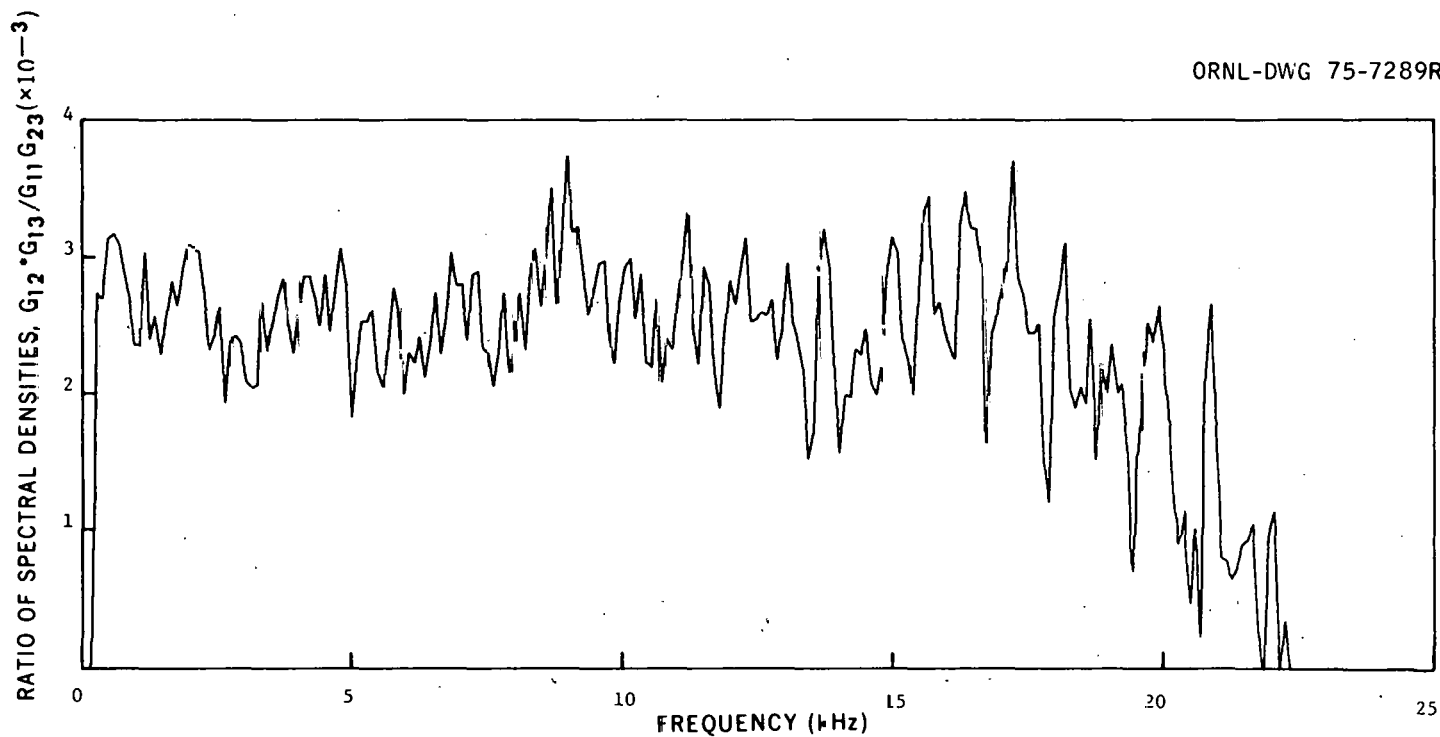
Fig. 13. Ratio of spectral densities $G_{12}^* G_{13} / G_{11} G_{23}$ as a function of frequency from the engineering mock-up core for FFTF with all fuel removed from rows 5 and 6 of trisector 3 and only control and safety rods of trisector 3 inserted (configuration 5).

The ratio of spectral densities given by Eq. (10) is independent of detection efficiency. To verify this prediction of the theory, measurements were performed for two assembly configurations with detectors of different efficiency. At 0.8 dollar subcritical (configuration 1), measurements were performed with both fission counters and the glass scintillators, resulting in a detection efficiency difference of a factor of $\sim$100. For the measurement at $\sim$30 dollars subcritical (configuration 2), the detection efficiency changes were produced by operating the scintillation system in both the current and pulse modes. In the pulse mode operation, the discriminator was set to reject $\sim$1/2 of the events, resulting in a change in detection efficiency of $\sim$2. The ratios of spectral densities $G_{12}^* G_{13}/G_{11}G_{23}$ (Table 1) are independent of detection efficiency and thus verify the prediction of Eq. (10) that this ratio of spectral densities is independent of detection efficiency.

Table 1. Ratio of spectral densities $G_{12}^* G_{13}/G_{11}G_{23}$ from measurements with ^{252}Cf in the mock-up core for the FFTF

Subcritical Reactivity (dollars)	Detector Type	Frequency (kHz)	$\dfrac{G_{12}^* G_{13}}{G_{11}G_{23}}$ ($\times 10^{-2}$)
$\sim$0.8	Fission	$\sim$0 – 8	0.0720
	Li (I)[a]	$\sim$0 – 8	0.0714
			0.0709[b]
			0.0715[b]
$\sim$30	Li (I)	$\sim$0 – 80	2.19
	Li (P)	$\sim$0 – 80	2.21

[a] (I) signifies operation of the scintillation system in the current mode, and (P) signifies operation of the scintillation system in the pulse mode, with the discriminator level set to reject half the events in the scintillator.

[b] Repeated measurements.

To verify that the number of detected events in the Li-glass scintillators in the core from neutrons directly from the ^{252}Cf source was negligible, the distance between the ^{252}Cf source and the scintillators was increased from 20 cm to 40 cm by moving the source 20 cm farther from the midplane of the core. The ratios of spectral densities and the cross-power spectral densities with ^{252}Cf themselves changed less than a few percent since the change in the value of I_c was also less than a few percent. Thus, the number of counts in the detectors from neutrons directly from the source was negligible compared to neutrons from fissions in the mock-up core.

3.7 Ratio of Importance Weighted Neutron Production Rates

The ratio of neutron production rates Y [Eq. (13)] was obtained from measurements of the ratio of count rates in fission counters located in the core and in all three shield mock-ups outside the radial reflector (Fig. 4). The ratio of the count rates with and without the ^{252}Cf source inserted is $(F_c I_c \bar{\nu}_c + F_i I_i \bar{\nu}_i)/F_i I_i \bar{\nu}_i$; it is equal to $Y/(Y - 1)$ and is given in Table 2 for several loadings of the engineering mock-up core. The measured values were between 2.04 and 1.72 for all core loadings (some of which were highly asymmetric) and detector locations, and, thus, they varied from the average value of 1.9 by at most only $\sim$10%.

4. EXPERIMENTS WITH A URANIUM METAL SPHERE

Experiments with an unreflected and unmoderated uranium (93.2 wt % ^{235}U) metal sphere, which has previously been studied in a series of time domain measurements using ^{252}Cf, were performed to further verify the theory of this ^{252}Cf noise analysis measurement. This sphere had the following advantages for this type of measurement: (1) the properties of the sphere required for the interpretation of this measurement had previously been measured in connection with time domain measurements,[23,31] (2) its geometry was simple and it was composed of a single homogeneous material, (3) it had a negligible inherent source, and (4) ^{6}Li-glass scintillators adjacent to the surface would have a high

detection efficiency because it is a small, high-leakage system and the scintillators are sensitive to gamma rays as well as neutrons. Items (1) and (2) simplified the interpretation of the results; item (3) allowed the use of existing small chambers containing ^{252}Cf which are well understood and have operated satisfactorily; item (4) permitted the measurements to be performed in a short time, <1 min of data sampling. One of the disadvantages of uranium metal assemblies for this type of measurement was that an independent accurate determination of the reactivity from breakfrequency noise analysis was not possible because the lowest breakfrequency from noise analysis for these systems in their most reactive condition is about 160 kHz, essentially beyond the capability of the Fourier analyzer due to the use of the anti-aliasing filter whose cutoff frequency was set at 70 kHz for these measurements. This also resulted in near-zero values of the imaginary part of G_{12}, thus making an accurate determination of the prompt-neutron decay constant from the ratio of the real to the imaginary part of G_{12} impractical.

Table 2. Results of measurements of $(F_c I_c \bar{\nu}_c + F_i I_i \bar{\nu}_i)/F_c I_c \bar{\nu}_c$ for the engineering mock-up core for the FFTF

Configuration[a]	In-Core	Ratio for Fission Counter Locations of LLFM			Average[b]
		TS-1	TS-2	TS-3	
1	1.89 (2.12)[c]	1.96 (2.04)	1.99 (2.01)	2.00 (2.00)	1.96 (2.04)
2	1.75 (2.33)	1.72 (2.38)	1.89 (2.12)	1.78 (2.28)	1.78 (2.28)
3	2.00 (2.00)	1.98 (2.02)	2.00 (2.00)	1.96 (2.04)	1.99 (2.01)
4	1.97 (2.04)	1.98 (2.02)	1.99 (2.01)	1.98 (2.03)	1.98 (2.02)
5[d]	1.77 (2.30)	1.70 (2.42)	1.94 (2.06)	1.89 (2.13)	1.81 (2.23)
6	1.98 (2.02)	1.93 (2.08)	2.04 (1.96)	2.00 (2.00)	1.99 (2.01)

[a]These configurations are described in Sect. 3.1 .

[b]The constancy of these values with loading configuration indicates that an inverse source neutron multiplication curve for the ^{252}Cf source has the same dependence on core loading as a similar curve for the inherent source neutron multiplication.

[c]Values in parentheses are the measured quantity, that is, the ratio of the count rate with the ^{252}Cf source inserted to that with it removed.

[d]Results given are for the source position closest to the midplane.

4.1 Description of the Sphere

The bare uranium (93.2 wt % ^{235}U) metal sphere of 8.744 cm radius consisted of three major sections (Figs. 14 and 15): a stationary central section suspended by four metal tubes, and remotely positioned upper and lower sections. The upper section was attached to a steel rod which was moved by a pneumatic cylinder. The lower section was attached to a low-mass aluminum support column which was mounted on the lift of a vertical assembly machine.[32] In the center section, a diametral hole could accommodate a ^{252}Cf chamber at the sphere center. Various-length split filler plugs of uranium could be placed around the 0.47-cm-diam shaft of the 1.27-cm-diam counter. Portions of or all of the holes could be filled with solid plugs.

Eight mass adjustment buttons with 44, 22, or 11 g each could be placed on the surface of the upper section and/or the lower section of the sphere. The average uranium density for the assembled sphere was 18.75 g/cm^3. A small aluminum (70 g) reflector for fine adjustment of reactivity was adjacent to a point on the lateral surface whose radius vector was perpendicular to the diametral hole. This reflector was mounted on an electric screw drive and could be positioned in contact with or up to 15 cm from the sphere surface. Two steel reflector pieces (293 and 447 g) could also be attached to the sphere surface to increase the reactivity.

4.2 Detectors and Instrumentation

The ^{252}Cf ionization chamber used in these measurements contained 0.07 µg of ^{252}Cf, corresponding to 41,000 spontaneous fissions per second. The pulse output of this detector after amplification (Fig. 16) and the counts as a function of discrimination level (Fig. 17) demonstrate that the ratio of minimum amplitude fission pulse to the maximum amplitude pulse from alpha particle decay is >3. This ratio was achieved by careful chamber design, and with the discriminator setting used, >99% of the ^{252}Cf fissions were detected. The auto-power spectral densities for operation in both the pulse and current modes are shown in Fig. 18. The
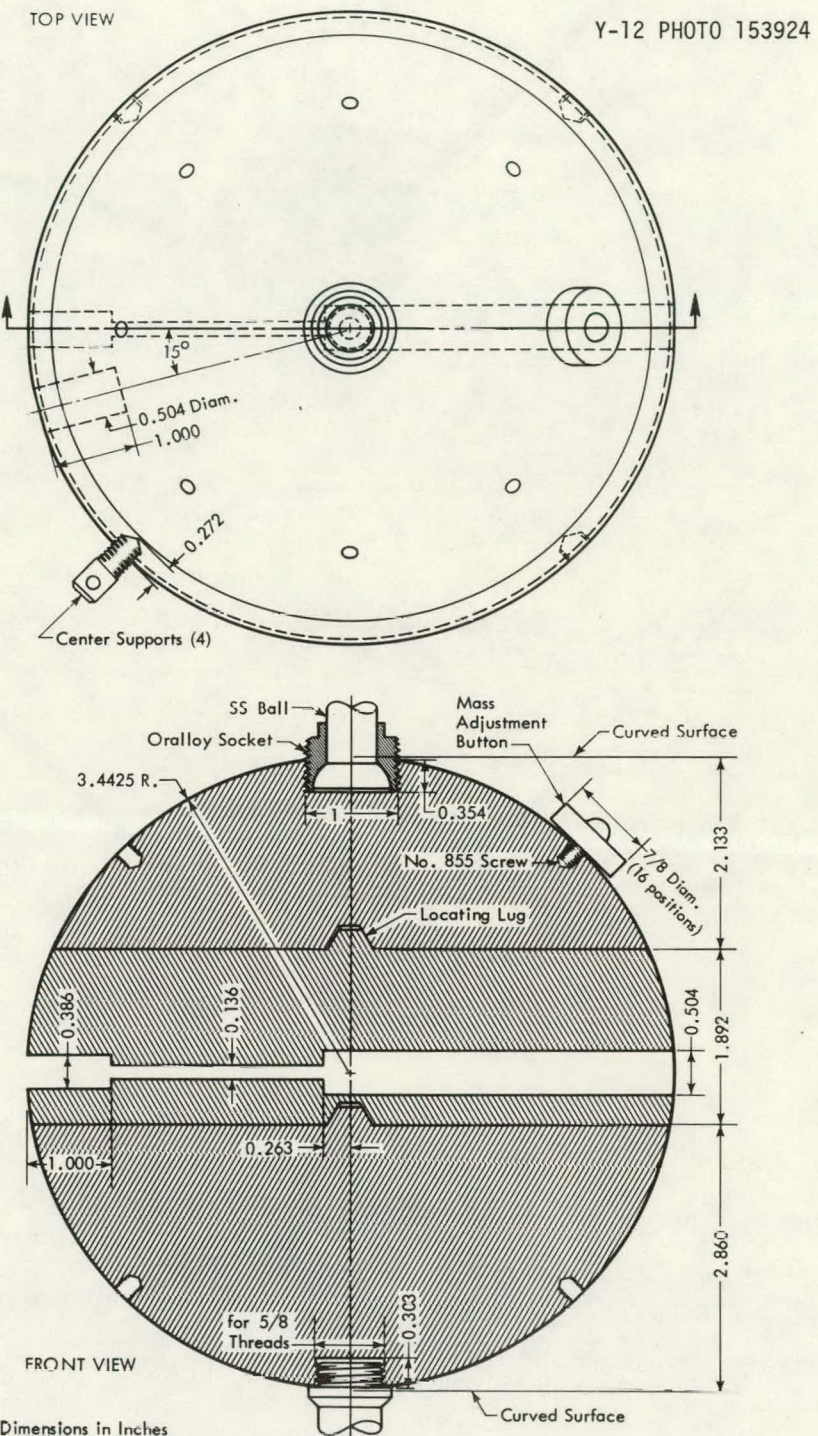
Fig. 14. Sketch of bare uranium sphere. Filler plugs were available for the 1-in.-deep hole on the surface and the diametral hole.
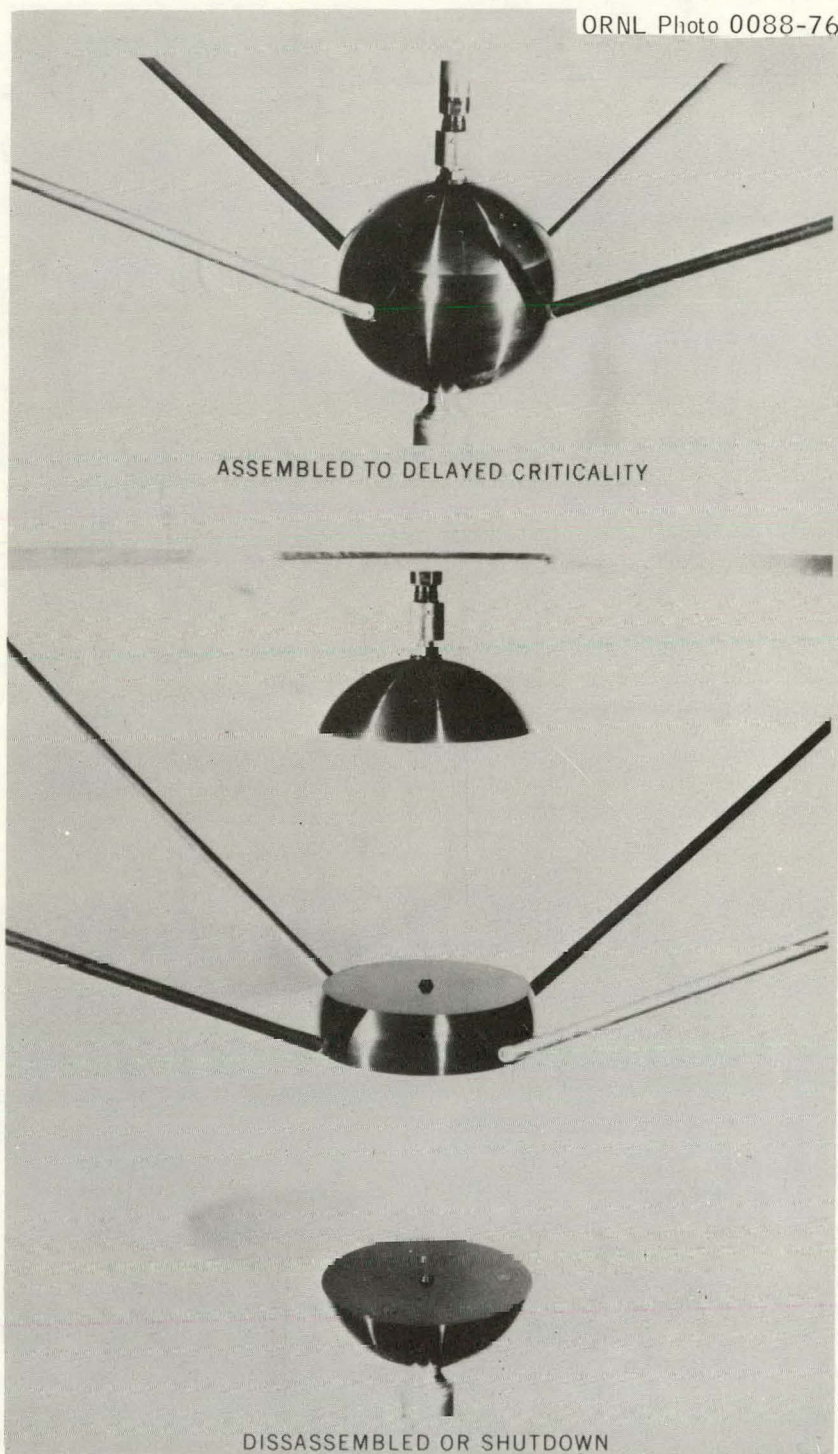
Fig. 15. Photograph of uranium sphere in assembled and disassembled conditions.
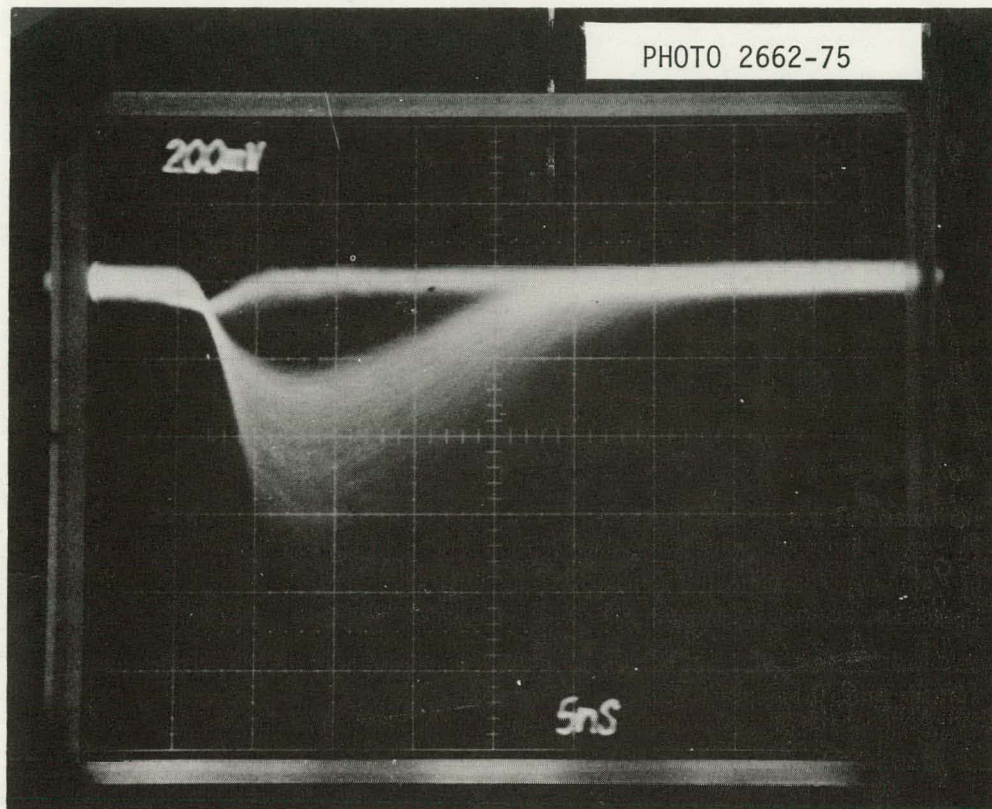
Fig. 16. Pulse output of ^{252}Cf chamber (0.07 µg) after amplification.
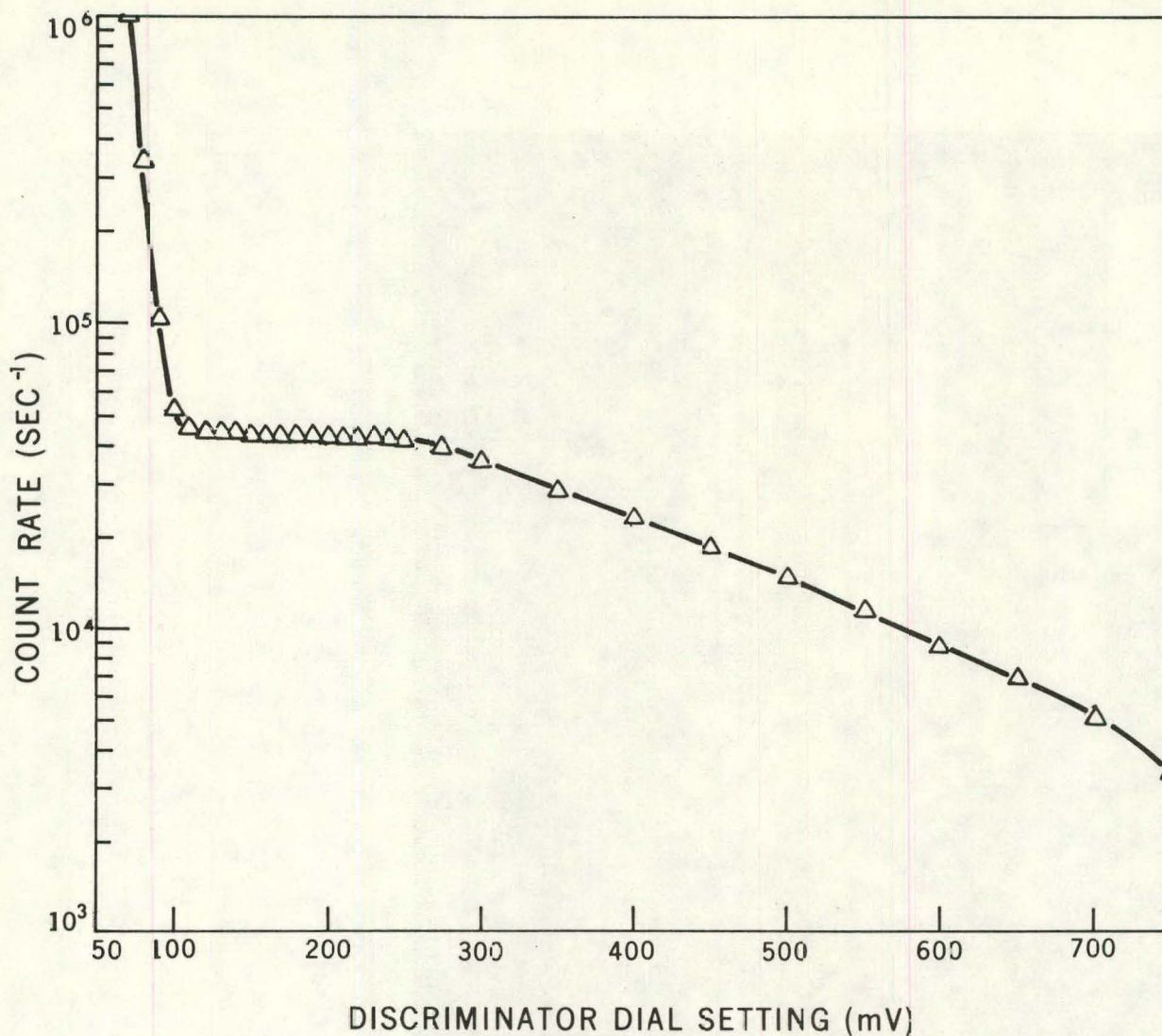
Fig. 17. Count rate vs discriminator setting fcr pulse mode operation of the ^{252}Cf (0.07 µg) ionization chamber used in the uranium metal sphere.
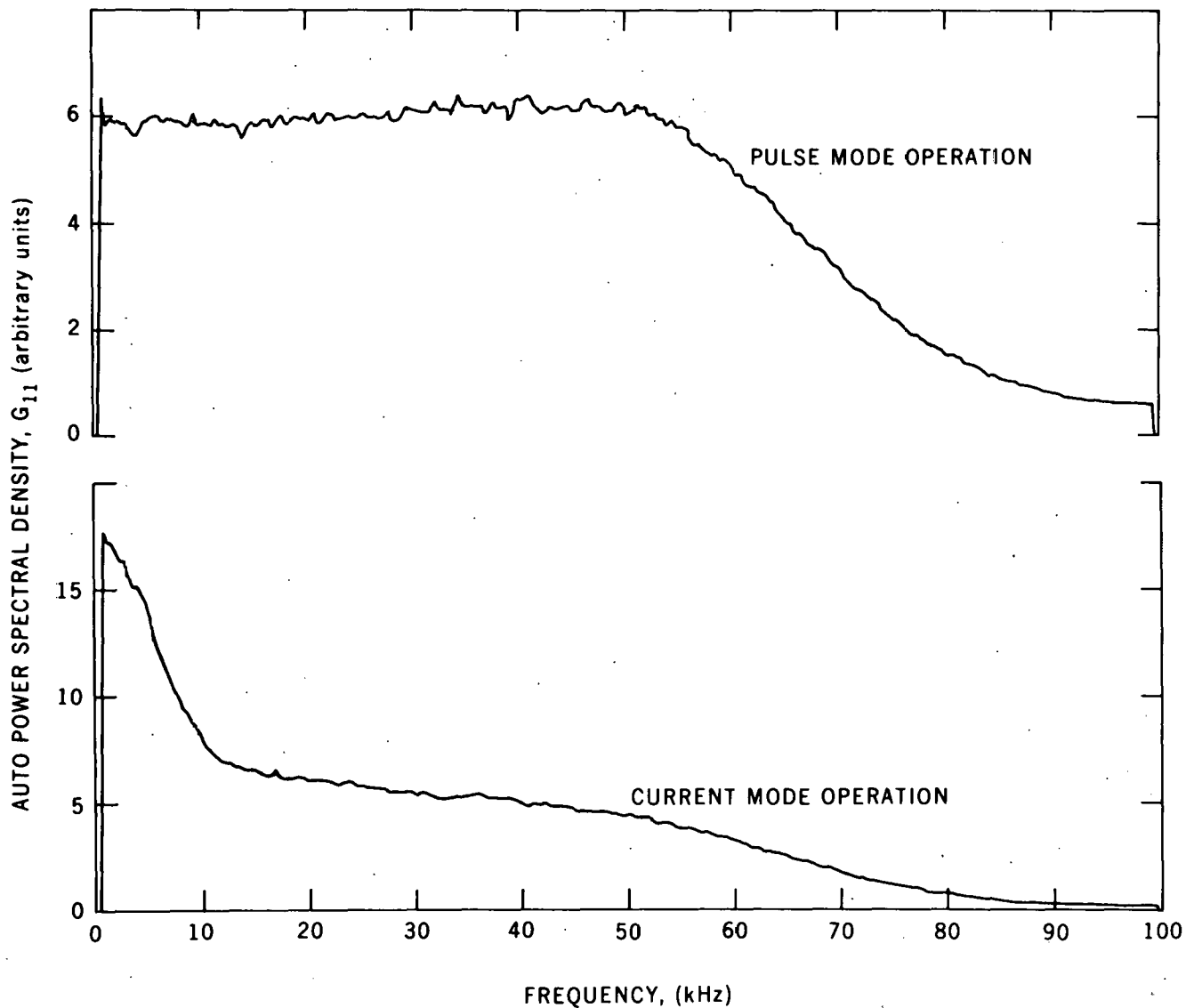
Fig. 18. Power spectral densities for the ^{252}Cf (0.07 μg) chamber operated in the pulse and current modes.

rolloff at 70 kHz is due to the setting of the anti-aliasing filter and that at low frequency in the current mode is due to the ion mobility in the chamber.

The ^{6}Li-glass scintillators, which had been used for measurements with the LMFBR mock-up, were used and were located in contact with the outer surface of the sphere. The instrumentation components and inter-facing of these detectors to the noise analyzer has previously been described.[26] At various times, measurements were also performed with 2.54-cm-diam, 2.54-cm-thick NaI scintillators and with the same photo-multipliers and electronics to verify that certain ratios of spectral densities were independent of detector type and efficiency.

4.3 Power Spectral Densities

Typical power spectral densities, corrected for the frequency response of the instrumentation, for a reactivity of 29 cents subcritical are shown in Fig. 19. In the figure, an auto-power spectral density (G_{c33}) of one of the ^{6}Li-glass scintillators, the cross-power spectral density (G_{c23}) between the two glass scintillators, and the square of the cross-power spectral density $(|G_{c13}|^2)$ between one of the scintillators and the ^{252}Cf chamber are plotted as a function of frequency up to 100 kHz. Since these spectral densities have been corrected for the frequency response of the instrumentation, the rolloff at high frequency is associated with the breakfrequency or decay constant of the sphere at this reactivity. The breakfrequencies of 165, 157, and 163 kHz determined in the least-squares fitting of the cross-power spectral densities are close to the expected breakfrequency for this assembly. The real and imaginary parts of the cross-power spectral density with ^{252}Cf are plotted as a function of frequency in Fig. 20. The near-zero values of the imaginary part at low frequencies, which is negative and proportional to $\omega/(\alpha^2 + \omega^2)$, changes linearly for $\omega \ll \alpha$, where $\alpha \approx 10^6$ sec^{-1}.

ORNL-DWG 75-12863R
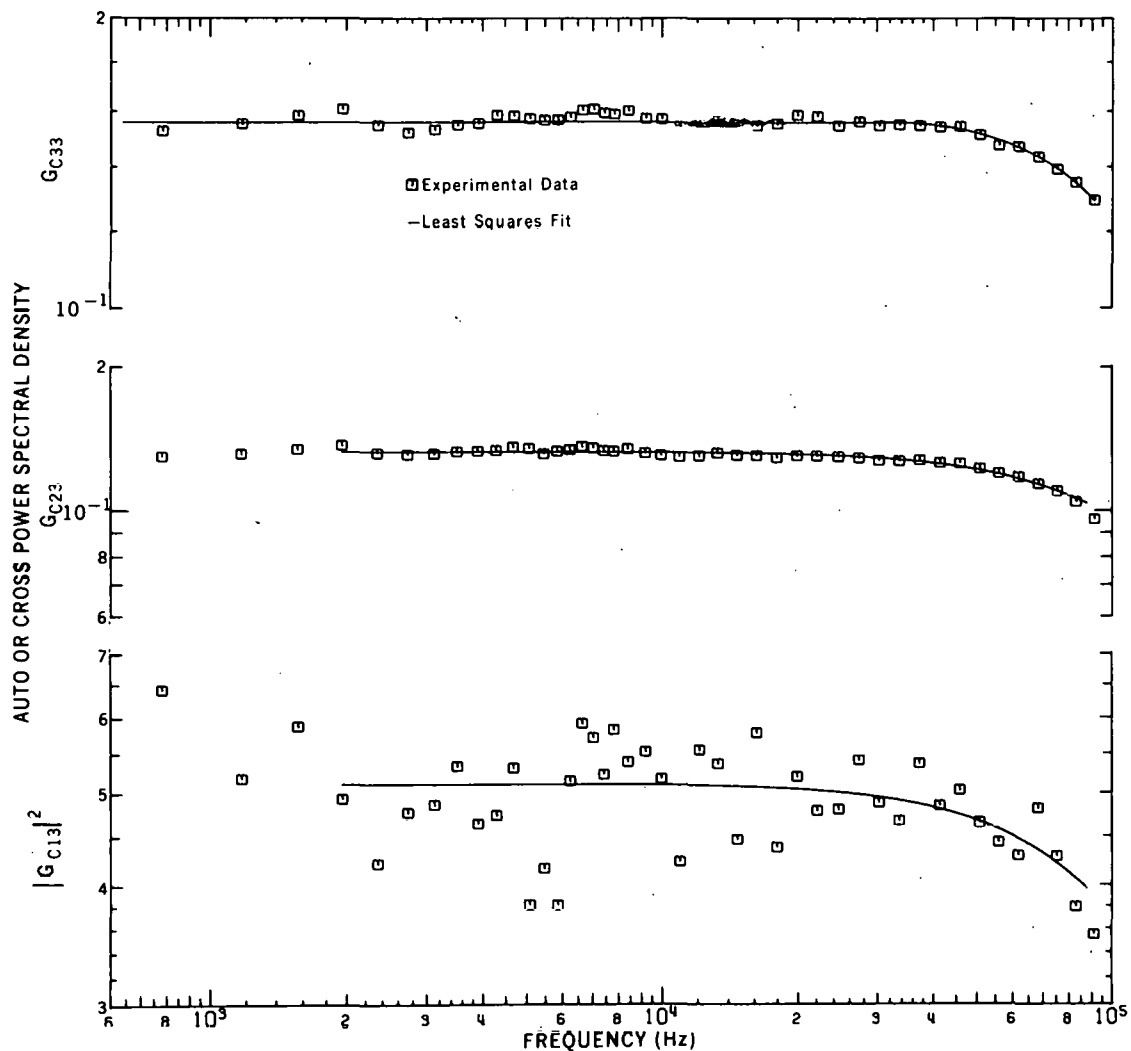
Fig. 19. Power spectral densities, G_{c33}, G_{c23}, and $|G_{c13}|^2$ for the uranium sphere with a reactivity of 29 cents subcritical.
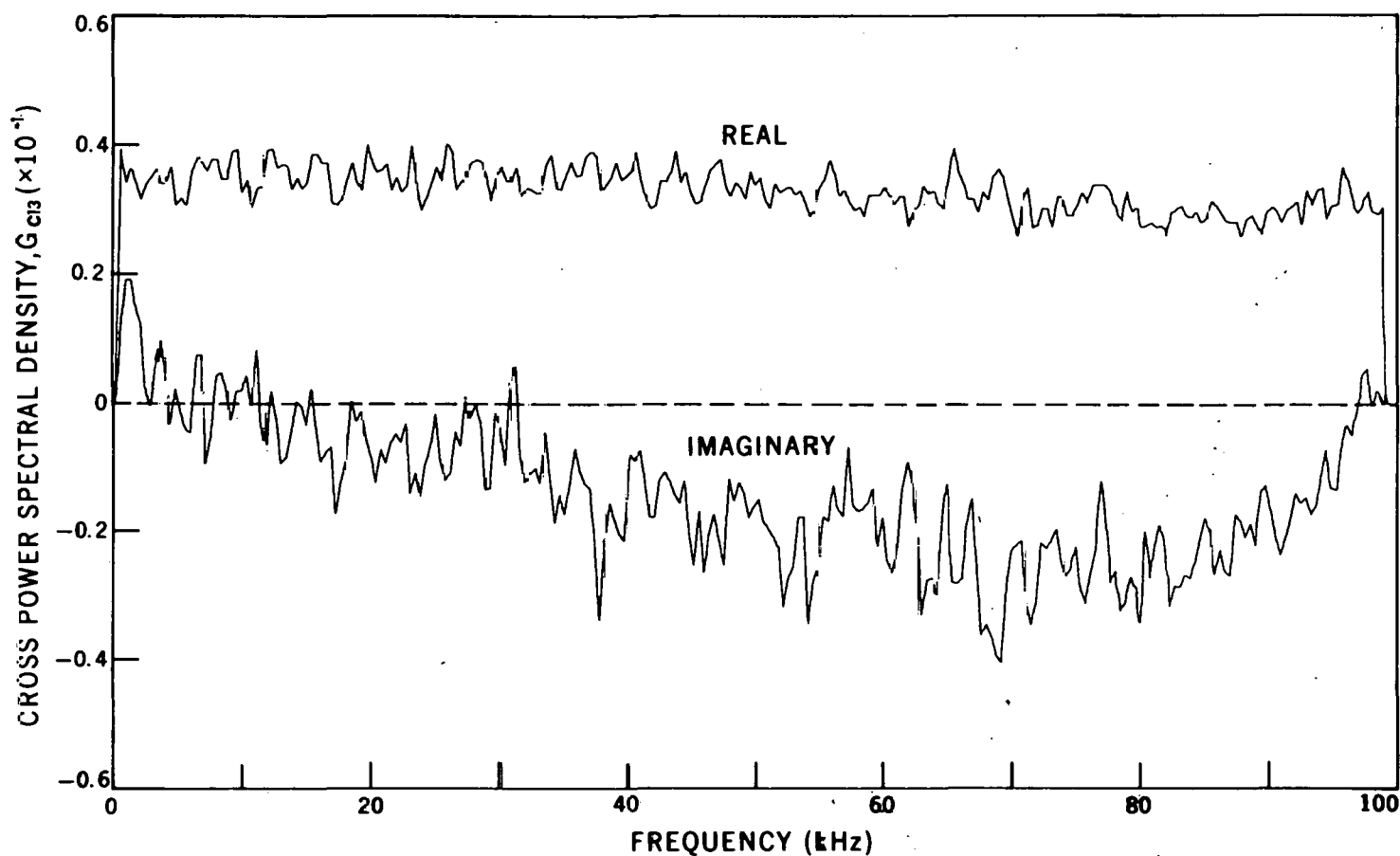
Fig. 2C. Cross-power spectral densities with ^{252}Cf, G_{c13}, for the uranium sphere with a reactivity of 29 cents subcritical.

4.4 Prompt-Neutron Decay Constant

The prompt-neutron decay constant is equal to the product of the frequency and the ratio of the real to the imaginary part of the cross-power spectral densities with ^{252}Cf. This product for the uranium sphere with a reactivity of 29 cents subcritical (Fig. 21) is constant between frequencies of 29 and 78 kHz and equal to 1.5 μsec^{-1}, whereas the value from other prompt-neutron decay constant measurements is 1.4 μsec^{-1}. The precision of this quantity is poor due to the errors in the imaginary part of the CPSD with ^{252}Cf, G_{12}, and is very poor at low and high frequencies due to the near-zero values of the imaginary part.

4.5 Coherence Amplitudes

The spectral densities were again combined to form the coherence amplitude as a function of frequency, and the result from the measurements with the sphere 29 cents subcritical are shown in Fig. 22. Because of the high neutron multiplication of the sphere, the coherence amplitude for the measurement with the two scintillators (0.77) is much larger than that from the measurements of the cross-power spectral density between one scintillator and the ^{252}Cf source (0.06).

4.6 Ratios of Spectral Densities

The ratio of spectral densities given by Eq. (10) is plotted in Fig. 23 as a function of frequency for the measurements with the sphere 29 cents subcritical. The average values of this combination of spectral densities, $G_{12}^{*}G_{13}/G_{11}G_{23}$, in various frequency ranges are also given in Table 3 for reactivities of 7, 29, and 250 cents subcritical. The independence of this ratio of frequency for the uranium metal sphere measurements again confirms this prediction of the theory.

The dependence of the ratio of spectral densities, $G_{12}^{*}G_{13}/G_{11}G_{23}$, on the ratio of importance weighted neutron production rates, $F_c I_c \nu_c / (F_i I_i \nu_i + F_c I_c \nu_c)$, was determined by measurements in which the
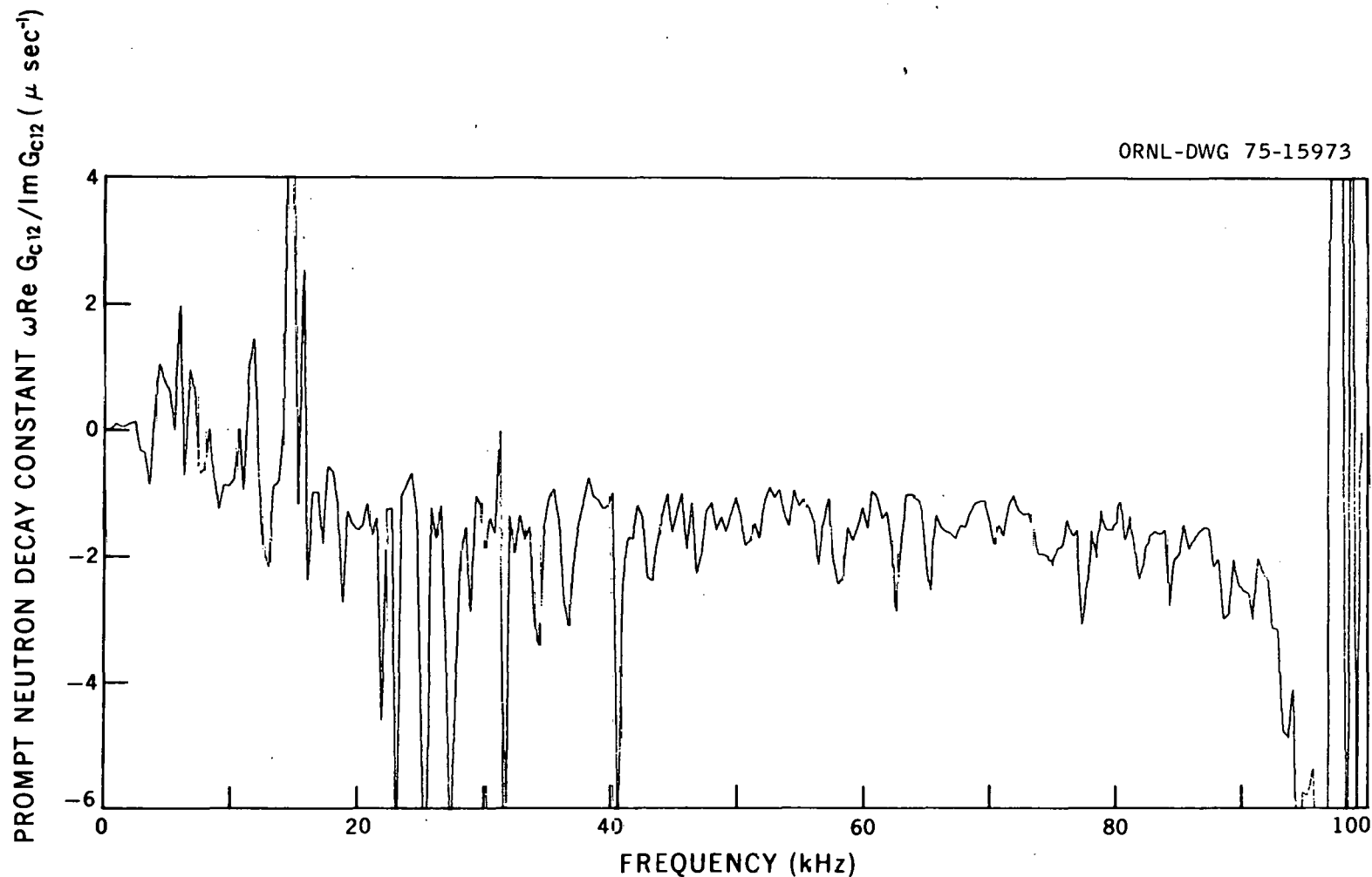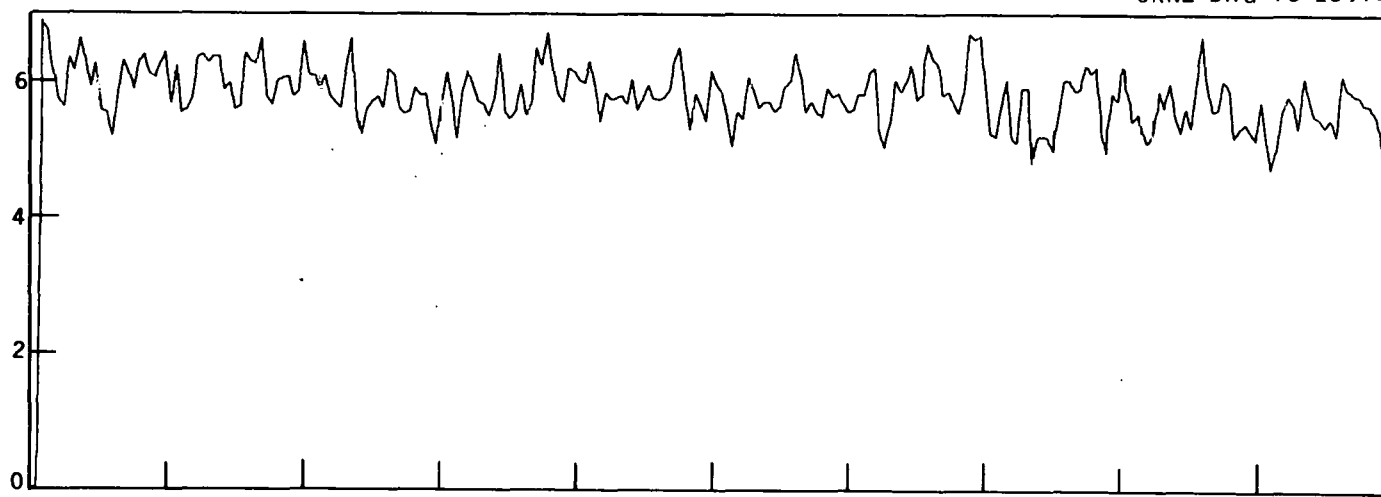
Fig. 21. Prompt-neutron decay constant, $\omega \mathrm{Re} G_{12}/\mathrm{Im} G_{12}$, vs frequency for the uranium sphere with a reactivity of 29 cents subcritical.

Fig. 22. Coherence amplitudes, γ_{13} and γ_{23}, for the uranium sphere with a reactivity of 29 cents subcritical.

ORNL-DWG 75-15974
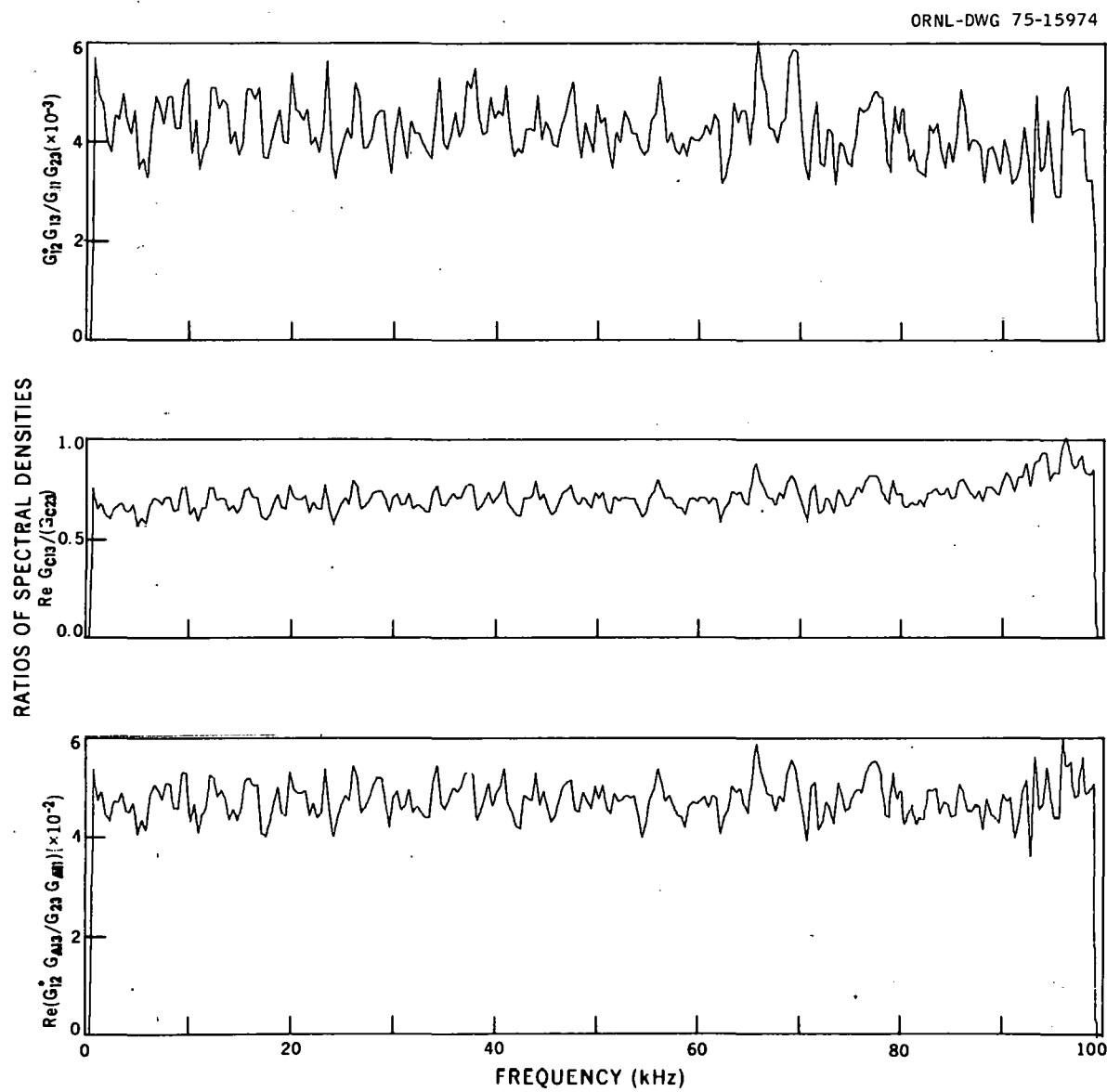
Fig. 23. Ratios of spectral densities for the uranium sphere with a reactivity of 29 cents subcritical.

^{252}Cf chamber was operated in the pulse mode. By raising the discrimination level in this pulse mode detection system, some of the spontaneous fissions of ^{252}Cf were not identified as initiators of fission chains. The rejected events in the ^{252}Cf chamber effectively acted as an inherent source, F_i, with the same neutron importance and number of neutrons per fission as neutrons from ^{252}Cf fission. Thus if D is the fraction of the spontaneous fissions of ^{252}Cf that were rejected by the discriminator, the ratio of importance-weighted neutron production rates, $F_c/(F_c + F_i)$, becomes $F_c(1 - D)/[F_c(1 - D) + F_cD]$ which equals $(1 - D)$. The value of D was varied from 0 to 0.8. The results of these measurements for the reactivity of the sphere $\sim$29 cents subcritical are given in Table 4 and Fig. 24. As predicted by theory, the ratio of spectral densities varies linearly with the fraction of fission chains identified as being initiated by neutrons from ^{252}Cf fission. Other ratios of spectral densities predicted by the theory (Fig. 23) to be independent of frequency were also formed from the spectral densities, and these values as a function of frequency and reactivity are also given in Tables 5 and 6.

Table 3. Ratio of spectral densities $G_{12}^*G_{13}/G_{11}G_{23}$ for the uranium sphere with reactivities of 7, 29, and 250 cents subcritical

Subcritical Reactivity (cents)	Ratio of Spectral Densities $G_{12}^*G_{13}/G_{11}G_{23}$ $(\times 10^{-4})$ for Frequency (kHz) of			
	0.8 - 9.8	9.8 - 19.5	19.5 - 29.3	29.3 - 39.0
7	10.8 ± 0.3	10.2 ± 0.8	11.5 ± 0.6	10.8 ± 0.6
29	44.0 ± 1.1	42.9 ± 1.1	43.0 ± 1.1	42.8 ± 1.1
250	404 ± 22	388 ± 27	388 ± 26	447 ± 29
	39.0 - 48.8	48.8 - 58.6	58.6 - 78.1	0.8 - 78.1
7	10.6 ± 0.7	10.6 ± 0.6	11.1 ± 0.4	10.9 ± 0.2
29	43.2 ± 0.9	41.6 ± 0.8	43.1 ± 0.9	43.0 ± 0.4
250	386 ± 24	408 ± 36	410 ± 27	400 ± 9

Table 4. Results of measurements in which the number of ^{252}Cf fissions identified as fission chain initiators was varied

Fraction of ^{252}Cf Fissions Rejected, D	$\dfrac{G_{12}^{*}G_{13}}{G_{11}G_{23}}$ ($\times 10^{-4}$)	Coherence Amplitude[a]			Standard Deviation for Various Spectral Densities,[b] %		
		γ_{12} ($\times 10^{-3}$)	γ_{13}[c] ($\times 10^{-2}$)	γ_{23}[d] ($\times 10^{-2}$)	$\mathrm{Re}\,G_{12}$	$\mathrm{Im}\,G_{12}$	G_{23}
0.0	37.9 ± 0.4	5.77 ± 0.03	5.28 ± 0.03	81.0 ± 0.1	10	10	3.0
0.22	28.2 ± 0.5	5.41 ± 0.05	4.81 ± 0.05	93.1 ± 0.1	12	11	3.2
0.41	21.7 ± 0.4	4.44 ± 0.04	4.01 ± 0.04	83.0 ± 0.9	13	13	3.0
0.60	15.0 ± 0.3	3.76 ± 0.04	3.33 ± 0.04	85.4 ± 1.1	10	15	2.9
0.81	7.6 ± 0.3	2.68 ± 0.04	2.36 ± 0.05	87.2 ± 1.0	20	21	2.8

[a]Coherence amplitude values at low frequency. Values are averaged over several frequencies to reduce uncertainty.

[b]Measurement and on-line processing time was 20 min.

[c]Slightly lower detection efficiency for detector 3 compared to detector 2 resulted in γ_{13} smaller than γ_{12}.

[d]Measurements were performed after a relatively high power operation. Sensitivity of the scintillators to gamma rays caused the value of γ_{23} to increase with time rather than remain constant. The order in which the measurements listed were performed was 1, 3, 4, 5, and 2, respectively.

ORNL-DWG 75-I2864Ri

FRACTION OF ^{252}Cf FISSIONS REJECTED BY THE DISCRIMINATOR

RATIO OF SPECTRAL DENSITYS. $G_{12}{}^* G_{13}/G_{11} G_{23}$ $(\times 10^{-4})$
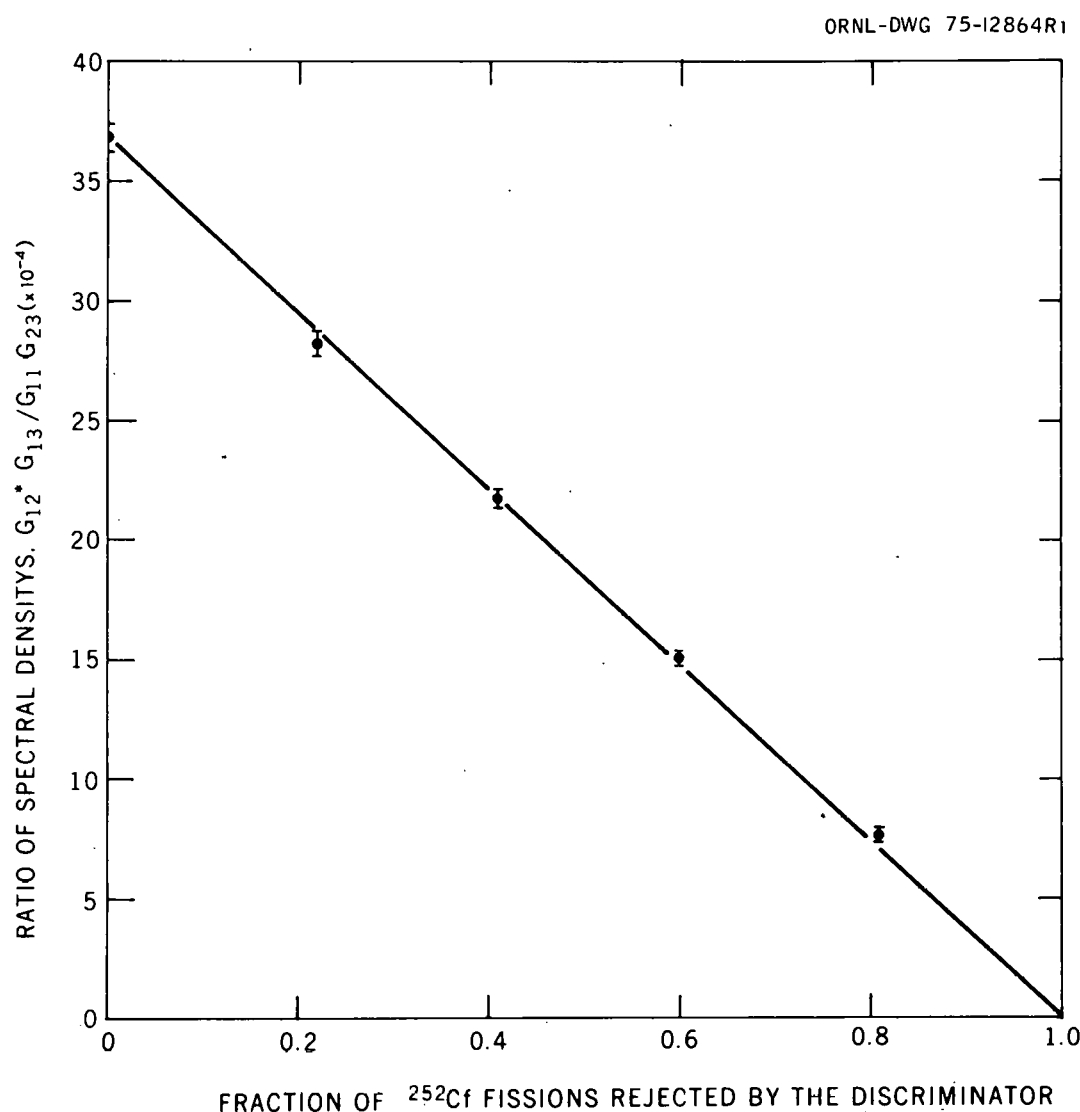
Fig. 24. Ratio of spectral densities, $G_{12}^* G_{13}/G_{11} G_{23}$ vs fraction of ^{252}Cf fissions rejected by the discriminator for the uranium sphere with a reactivity of 29 cents subcritical.

Table 5. ReG_{c12}/G_{c23} and ReG_{c13}/G_{c23} in various frequency intervals for the uranium sphere with reactivities of 7, 29, and 250 cents subcritical

Subcritical Reactivity (cents)	Ratio of Spectral Densities ($\times 10^{-3}$) for Frequency (kHz) of[a]			
	0.8 – 9.8	9.8 – 19.5	19.5 – 29.3	29.3 – 39.1
7	14.2 ± 0.5	15.3 ± 0.4	14.8 ± 0.5	14.6 ± 0.5
	13.3 + 0.6	14.9 + 0.4	14.4 ± 0.5	14.6 ± 0.5
29	71.0 ± 1.0	71.3 ± 0.7	69.2 ± 0.8	69.5 ± 0.9
	65.5 ± 1.1	66.1 ± 0.9	68.3 ± 1.0	68.3 ± 0.9
250	2190 ± 100	2220 ± 150	2420 ± 150	2630 ± 180
	2010 ± 120	2220 ± 160	2270 ± 100	2730 ± 150
	39.1 – 48.8	48.8 – 58.6	58.6 – 78.1	0.8 – 78.1
7	14.6 ± 0.5	15.1 ± 0.4	15.6 ± 0.4	15.1 ± 0.2
	14.7 ± 0.4	15.2 ± 0.3	15.4 ± 0.4	14.7 ± 0.2
29	70.4 ± 0.6	69.2 ± 0.8	72.2 ± 0.8	70.1 ± 0.3
	68.6 ± 0.9	67.9 ± 0.9	70.5 ± 0.9	67.4 ± 0.4
250	2140 ± 110	2680 ± 190	2410 ± 120	2390 ± 60
	2720 ± 150	2750 ± 220	2410 ± 130	2440 ± 60

[a]Entries on the first line for each reactivity are ReG_{c12}/G_{c23}, while those on the second line are ReG_{c13}/G_{c23}.

Table 6. Real parts of $G^*_{12}G_{A13}/G_{23}G_{A11}$ and $G^*_{A12}G_{13}/G_{A11}G_{23}$ in various frequency intervals for the uranium sphere with reactivities of 7, 29, and 250 cents subcritical

Subcritical Reactivity (cents)	Ratio of Spectral Densities ($\times 10^{-3}$) for Frequency (kHz) of[a]			
	0.8 – 9.8	9.8 – 19.5	19.5 – 29.3	29.3 – 39.1
7	10.4 ± 0.4	11.0 ± 0.3	10.7 ± 0.3	10.5 ± 0.4
	9.7 ± 0.4	10.6 ± 0.3	10.3 ± 0.3	10.4 ± 0.4
29	50.8 ± 0.7	49.5 ± 0.5	48.3 ± 0.5	48.0 ± 0.7
	46.8 ± 0.7	56.0 ± 0.7	47.5 ± 0.7	47.2 ± 0.7
250	1590 ± 70	1530 ± 100	1670 ± 90	1870 ± 130
	1450 ± 90	1540 ± 120	1560 ± 70	1951 ± 110
	39.1 – 48.8	48.8 – 58.6	58.6 – 78.1	0.8 – 78.1
7	10.4 ± 0.3	10.8 ± 0.3	11.0 ± 0.3	10.7 ± 0.1
	10.4 ± 0.3	10.7 ± 0.2	10.6 ± 0.3	10.4 ± 0.1
29	48.4 ± 0.5	47.7 ± 0.5	49.2 ± 0.5	48.9 ± 0.2
	47.1 ± 0.6	46.7 ± 0.6	48.0 ± 0.6	47.2 ± 0.3
250	1520 ± 80	1810 ± 140	1650 ± 83	1660 ± 40
	1780 ± 90	1800 ± 140	1650 ± 95	1670 ± 40

[a]Entries of the first line for each reactivity are $Re(G^*_{12}G_{A13}/G_{23}G_{A11})$, while those on the second line are $Re(G^*_{A12}G_{13}/G_{A11}G_{23})$.

4.7 Determination of $B_c(1 + C_\alpha)$ and $\overline{v_c^2} \Big/ \overline{v}_c^2$

Performance of the measurement of the ratio of spectral densities, $G_{12}^{*}G_{13}/G_{11}G_{23}$, for both current and pulse mode operation of the chamber containing the ^{252}Cf allowed the determination of the quantity $B_c(1 + C_\alpha)$, since for pulse mode operation this quantity does not appear in Eq. (10). The ratio of this combination of spectral densities for pulse mode operation of the ^{252}Cf chamber to that for current mode operation is equal to $B_c(1 + C_\alpha)$, since all other quantities in Eq. (10) remain unchanged. Several pairs of measurements were made at various reactivities to determine this ratio, which can be compared to calculations. Measurements were performed for both the sphere and cylinder and also in the calibration where the frequency response of the scintillation detection systems was measured (Table 7). These calibration measurements were performed with the ^{252}Cf chamber between the two scintillators with no other significant materials near the detectors. The average value of $B_c(1 + C_\alpha)$ is 1.16 ± 0.07 for the 0.95-cm-diam annular chamber, while that for the 1.27-cm-diam, parallel-plate chamber is 1.367 ± 0.014. These values can be compared to those predicted by Allen (ref. 33) who used the chamber geometry to calculate from basic data the value of the average square of the charge produced by an alpha particle decay or spontaneous fission, and the square of the average charge from spontaneous fission in the chamber. The calculated values of the factor $B_c(1 + C_\alpha)$ were 1.53 and 1.63 for the annular and parallel-plate chambers, respectively. The values, calculated from basic data and the chamber geometry, differ by 32 and 20% from those measured for the annular and parallel-plate chambers, respectively.

If the ratio of spectral densities $G_{A12}^{*}G_{A13}/G_{A11}G_{A23}$ is obtained from the calibration measurements, it can be shown theoretically to equal

$$\frac{1}{B_c(1 + C_\alpha)} \frac{\overline{v}_c^2}{\overline{v_c^2}} \; ;$$

and for pulse mode electronics where all the alpha particle decays of ^{252}Cf can be discriminated against, it is equal to $\overline{\nu_c^2}\big/\overline{\nu_c^2}$ since $B_c(1 + C_\alpha) = 1$. Thus, the ratio of spectral densities in both modes of operation for the calibration measurements will also determine the value of $B_c(1 + C_\alpha)$ since the ratio $\overline{\nu_c^2}\big/\overline{\nu_c^2}$ is known from other measurements.[34] Since this measurement involves only the detectors, it is the most accurate and simple way of determining the value of $B_c(1 + C_\alpha)$, and these values are also presented in Table 7.

Table 7. Values of $B_c(1 + C_\alpha)$ for the annular
and parallel-plate ionization chambers
with ^{252}Cf

Configuration	Nominal Subcritical Reactivity (dollars)	$B_c(1 + C_\alpha)$
Annular Chamber[a]		
Sphere	0.09	1.16 ± 0.07
Parallel-Plate Chamber[b]		
Sphere	0.29	1.36 ± 0.04
		1.43 ± 0.04
		1.23 ± 0.04
		1.40 ± 0.07
		1.38 ± 0.07
		1.34 ± 0.07
Cylinder	0.5	1.30 + 0.04
Cylinder	4.4	1.37 ± 0.02
Cylinder	6.1	1.34 ± 0.05
Cylinder	7.9	1.31 ± 0.04
Calibration	--	1.38 ± 0.01
Calibration	--	1.41 ± 0.01
	Average	1.37 ± 0.01

[a]0.95-cm-diam chamber.

[b]1.27-cm-diam chamber.

Since for pulse mode operation of the ^{252}Cf chamber, the ratio of spectral densities can be used to obtain the value of $\overline{\nu_c^2} \big/ \overline{\nu_c^2}$ which is known from independent direct measurements of the number of neutrons per fission, good agreement between this determination of $\overline{\nu_c^2} \big/ \overline{\nu_c^2}$ and independent measurements is an excellent way of checking the accuracy and correctness of the Fourier analyzer processing (both hardware and software) as well as the proper operation of the detection systems. The values of $\overline{\nu_c^2} \big/ \overline{\nu_c^2}$ obtained from two calibration measurements with the ^{252}Cf chamber operating in the pulse mode are 0.891 ± 0.002 and 0.905 ± 0.007, whereas the value from previous direct measurement of the number of neutrons per fission is 0.899.[34] This good agreement confirms the correctness of the data accumulation processing and analysis by the total noise analysis system.

Since $\overline{\nu_c^2} \big/ \overline{\nu_c^2}$ is known very accurately from other measurements, the calibration measurement for the frequency response of the system can be used to determine the values of $B_c(1 + C_\alpha)$. In implementing this method to determine the reactivity in a reactor application, the value of $B_c(1 + C_\alpha)$ should be determined from the calibration run and this value should be employed in Eq. (11) to determine the reactivity for the measurements with a reactor.

4.8 Independence of $G_{12}^* G_{13}/G_{11} G_{23}$ of Detection Efficiency

The independence of the ratio of spectral densities $G_{12}^* G_{13}/G_{11} G_{23}$ of the detection efficiency was verified in comparison measurements in which the detection efficiency was changed in a variety of ways. It was varied in the measurements with the sphere by operating the Li-glass scintillator system in both the current and pulse mode. This resulted in a 62% change in the detection efficiency, while the ratio changed only 4%. The detection efficiency was also varied by substituting a NaI scintillator (2.54 cm high, 2.54 cm diam) for the Li-glass scintillator. The NaI was sensitive only to gamma rays, while the Li glass was sensitive to both gamma rays and neutrons. Thus, not only was the detection efficiency (counts/reactor fission) changed, but also the type

of particles detected. The detection efficiency was changed also by moving the Li-glass detector from contact with the sphere surface to 4.5 cm away. For all changes, the reactivity was reproduced by adding surface mass adjustment buttons or the aluminum reflector until the sub-critical power level was the same after the change as before. The results of these measurements, given in Table 8, show that, as in the experiments with the mock-up core for the FFTF, this ratio of spectral densities is independent of detection efficiency.

4.9 Reactivity from the Ratio $G_{12}^{*}G_{13}/G_{11}G_{23}$

The reactivity can be obtained from the measurement of the ratio of spectral densities $G_{12}^{*}G_{13}/G_{11}G_{23}$ if the other quantities in Eq. (12) are known. One of the principal reasons for performance of these measure-ments with the sphere was the knowledge of these quantities from other measurements which were performed previously to investigate the applica-tion of this method in the time domain.[23,35] The values of these quanti-ties will be summarized in this section, and the reactivities determined using them will be compared with independent measurements.

Table 8. Independence of detection efficiency for the ratio of spectral densities $G_{12}^{*}G_{13}/G_{11}G_{23}$

Assembly	Change in Detection Efficiency (%)	Change in $G_{12}^{*}G_{13}/G_{11}G_{23}$ (%)	Detection Efficiency Change Resulting From
Sphere	+62	+4	pulse to current mode operation of Li-glass scintillator
Sphere	+22	-14	NaI to Li-glass detectors
Sphere	-26	-1	movement away from sphere surface of Li glass
Cylinder, 12.07 cm high	+340	+6	NaI to Li-glass detectors
Cylinder, 11.75 cm high	-125	-5	Pb shield between NaI and cylinder surface

4.9.1 Value of Y

The ratio of fission chains initiated by neutrons from an inherent plus a ^{252}Cf source to those initiated by neutrons from the ^{252}Cf sources, Y [Eq. (13)], equals unity for these measurements since there is no significant inherent source in the uranium sphere assembly. In these measurements the only exception to this was discussed in Sect. 4.6.

4.9.2 Value of P_1

The value of P_1 [Eq. (14)] for pulse mode operation of the ^{252}Cf chamber simplifies to $RXI\bar{\nu}/I_c\bar{\nu}_c$ since the value of $B_c(1 + C_\alpha)$ equals unity. The average number of prompt neutrons per fission of ^{252}Cf, $\bar{\nu}_c$, used in the interpretation of the measurement, 3.7224 ± 0.0081, is the reevaluated weighted mean of DeVolpi,[36] 3.731 ± 0.008, minus the number of delayed neutrons per fission from Cox,[37] 0.0086 ± 0.0001. The average number of prompt neutrons per reactor fission, $\bar{\nu}$, was obtained by using the fluxes from transport theory calculations[38] and the ENDF/B-III[39] data to calculate the total number of neutrons per reactor fission, which was 2.597. The number of delayed neutrons per reactor fission was obtained with the delayed-neutron yields[40-42] and the delayed-neutron effectiveness calculations using the forward and adjoint fluxes from S_n transport theory calculations and the delayed-neutron spectra of Bachelor.[43] The effective delayed-neutron fraction calculated in this way is 0.0066. Thus, the number of prompt neutrons per fission is 2.580.

The importance of the neutrons from the spontaneous fission of ^{252}Cf in the ionization chamber was obtained from previous measurements which compared the source neutron multiplication of the slightly subcritical sphere with the ^{252}Cf chamber installed with that for the sphere at the same reactivity but with a point source in the center. This measured value is 0.9117 ± 0.0037[35] for the parallel-plate chamber in the center of the diametric hole and 0.4379 ± 0.0065 for the annular chamber in the hole at the outer surface of the sphere. The average value of the neutron importance of fission neutrons was obtained from the measured neutron importance and fission density distribution by averaging the neutron importance over the sphere value using the fission density as a weighting function. The resulting value is 0.5633 ± 0.0003 (ref. 35).

The value of the Diven factor, $X = \overline{\nu(\nu - 1)}\big/ \bar{\nu}^2$, was obtained by averaging the value of $\nu(\nu - 1)$ and ν over the sphere volume using the fission density obtained from transport theory calculations with the ENDF/III-B cross sections as a weighting function. The result obtained, 0.805, is consistent with the previously measured value of Diven.[44]

The value of the factor, R (1.123), which is introduced into the point kinetics equations to account for spatial effects was obtained from measured fission densities and neutron importance distributions.[35] Combining the above quantities by using Eq. (14) gives a value for P_1 equal to 0.387.

4.9.3 Values of P_2 to P_5

The expression for P_2 [Eq. (15)] for this assembly in which there is a negligible inherent neutron source reduces to $\left(\overline{\nu_c^2}\big/\bar{\nu}_c\right)\big/ XRY$. The value of $\overline{\nu_c^2}$ is obtained from the measurements of Boldeman[34] and is equal 15.541 ± 0.006. With the resulting value of $P_2 = 4.62$ and a value of P_3 of 5.7×10^{-3}, the values of P_4 and P_5 are obtained.

4.9.4 Reactivity Values

Using these values and the ratio of spectral densities, the reactivity of the uranium sphere was determined. The results are compared in Table 9 with other measurements. The values in the other measurements were determined from stable reactor period measurements, from removal of calibrated surface mass adjustment buttons, or by inverse kinetics rod drop measurements in which the lower section was displaced slightly from the central section of the sphere. The values determined are in good agreement with the value from independent measurements for reactivities close to delayed criticality. For the configurations of the sphere with the top section removed slightly, the reactivities are not in as good agreement with other measurements. For these configurations, the values of I and I_c used were those for the configuration with the top section of the sphere in contact with the central section. Thus, the disagreement in the reactivities could be the result of using values of I and I_c for a different configuration (the fully assembled one).

Table 9. Reactivity determinations from $G^*_{12}G_{13}/G_{11}G_{23}$ for the uranium sphere for pulse mode operation of the ^{252}Cf chamber

| Detector | ^{252}Cf Chamber | $\dfrac{G^*_{12}G_{13}}{G_{11}G_{23}}$ ($\times 10^{-4}$) | Subcritical Reactivity (cents) | | |
| | | | Other Methods | Noise Analysis | |
				Measured Values	Average
Li	Parallel-plate	10.6 ± 0.3	7.0[a]	6.3 ± 0.2	6.7 ± 0.2
		11.9 ± 0.4		7.0 ± 0.2	
Li	Annular	6.9 + 0.6	8.8[a]	8.5 ± 0.9	8.5 ± 0.3
		6.8 ± 0.3		8.5 ± 0.4	
		7.2 ± 0.3		8.9 ± 0.4	
		6.6 ± 0.2		8.2 ± 0.2	
NaI	Parallel-plate	48.2 ± 0.8	29[b]	28.5 ± 0.5	27.5 ± 0.8
		46.8 ± 0.8		27.7 ± 0.5	
		45.9 ± 0.8		27.2 ± 0.5	
		48.2 ± 0.8		28.5 ± 0.5	
		45.2 ± 0.8		26.7 ± 0.5	
		44.9 ± 0.8		26.6 ± 0.5	
Li	Parallel-plate	41.6 ± 0.7	29[b]	24.6 ± 0.4	25.0 ± 1.2
		41.7 ± 0.8		24.7 ± 0.4	
		42.2 ± 0.7		24.9 ± 0.4	
		42.7 ± 0.8		25.3 ± 0.4	
		42.0 ± 0.7		24.9 ± 0.4	
		44.8 ± 0.7		26.5 ± 0.4	
		43.2 ± 0.8		25.6 ± 0.4	
		42.9 ± 0.7		25.6 ± 0.4	
		36.7 ± 0.6		21.7 ± 0.4	
		40.6 ± 0.6		24.7 ± 0.4	
Li	Parallel-plate	428 ± 12	230[c]	260 ± 7	260 ± 7
Li	Parallel-plate	410 ± 31	240[c]	249 ± 18	249 ± 18

[a]This value was determined from stable reactor period measurements.

[b]This value was obtained by removal of calibrated surface mass adjustment buttons.

[c]These values were determined by inverse kinetics rod drop measurements in which the lower section of the sphere was displaced slightly from the central section.

5. EXPERIMENTS WITH URANIUM METAL CYLINDERS

It was desirable to perform measurements with small uranium metal assemblies at lower reactivities to verify the theory of this type of measurement. To reduce the reactivity further by the removal of the top section of the sphere assembly would have resulted in a complicated three-dimensional system for which it would be difficult to calculate the quantities required to interpret this type of measurement. Unreflected and unmoderated uranium cylinders had previously been assembled and the reactivity calibrated as a function of height by both the pulsed neutron and inverse kinetics rod drop techniques down to about 30 dollars sub-critical.[45] These previously measured values of the reactivity agreed with each other and with direct calculation of the reactivity, assuming that the value of the effective delayed-neutron fraction was 0.0066. Since the calculated fission density and neutron importance distribution for the bare sphere agreed very well with measurements, transport theory calculations of these distributions should be adequate for two-dimensional cylindrical assemblies of the same material. Since the parallel-plate ionization chamber was cylindrically symmetrical, it could be modeled rather precisely for the calculation of the importance of neutrons from spontaneous fission of ^{252}Cf in the counter.

Noise analysis measurements were performed for uranium metal cylin-ders, and the reactivities determined by this method are compared with the previously measured values. The verification of various predictions of the theory was also made from the data from these measurements.

5.1 Description of the Uranium Metal Cylinders

The uranium metal[46] available for these experiments was enriched to 93.15 wt % in the ^{235}U isotope and had an average density of 18.76 g/cm^3. Individual pieces were in the form of 17.77-cm-diam disks varying in thickness from 0.32 to 3.81 cm. The available thicknesses were such that the assembly heights could be altered in 0.16-cm steps. The pieces were fabricated with a ±0.005-cm variation in any dimension, and a total vari-ation in flatness of <0.005 cm. The cylinder height was varied from 5.10

to 12.54 cm. For the assemblies near delayed criticality, the assembly
was made up of two sections, a lower section as well as the upper section.
As shown in Fig. 25, the upper section of each assembly was built on a
0.025-cm-thick, stainless-steel diaphragm held in position by a 76-cm-ID,
2.5-cm-thick aluminum clamping ring. The lower section was supported on
a low-mass aluminum stand, the assembly being completed when the lower
section was raised by a 61 cm stroke of a piston. The apparatus for
these assemblies has previously been described.[32] Also shown in the
figure is the location of the parallel-plate ^{252}Cf chamber in the center
of the upper flat surface of the cylinder and that of two ^{6}Li-glass scin-
tillators adjacent to the radial surface approximately at the midplane.
For some measurements, NaI scintillators sensitive to gamma rays were
also used. These were the same detectors used for the sphere measurements.

5.2 Previous Reactivity Determinations

The reactivity was determined using previous measurements of the
prompt-neutron decay constants: the decay constant at delayed critical-
ity (1.082 μsec^{-1}),[46] and those measured for cylinder heights from 12.22
to 8.28 cm. Changes in the prompt-neutron lifetime from the delayed
critical cylinder to cylinders of the various heights (from S_n transport
theory calculations) were used with the measured decay constants to
obtain the subcritical reactivity. The reactivity was also obtained from
the calculated neutron multiplication factor, using a value of the effec-
tive delayed-neutron fraction of 0.0066. The results of these calcula-
tions are compared with previous measurements in Table 10. The close
agreement of these measured and calculated reactivities as well as those
for 27.9-cm-diam and 38.1-cm-diam uranium metal cylinders[45] shows that
the reactivity as a function of cylinder height is accurately known. This
functional dependence of subcritical reactivity on cylinder height was
interpolated to obtain the reactivities for the cylinder heights of this
experiment, which were corrected for the reactivity effect of detectors
($\sim$52 cents). These reactivities (Table 11) and the reactivity values
from noise analysis will be compared to verify the noise methods.

252Cf Source

Detectors
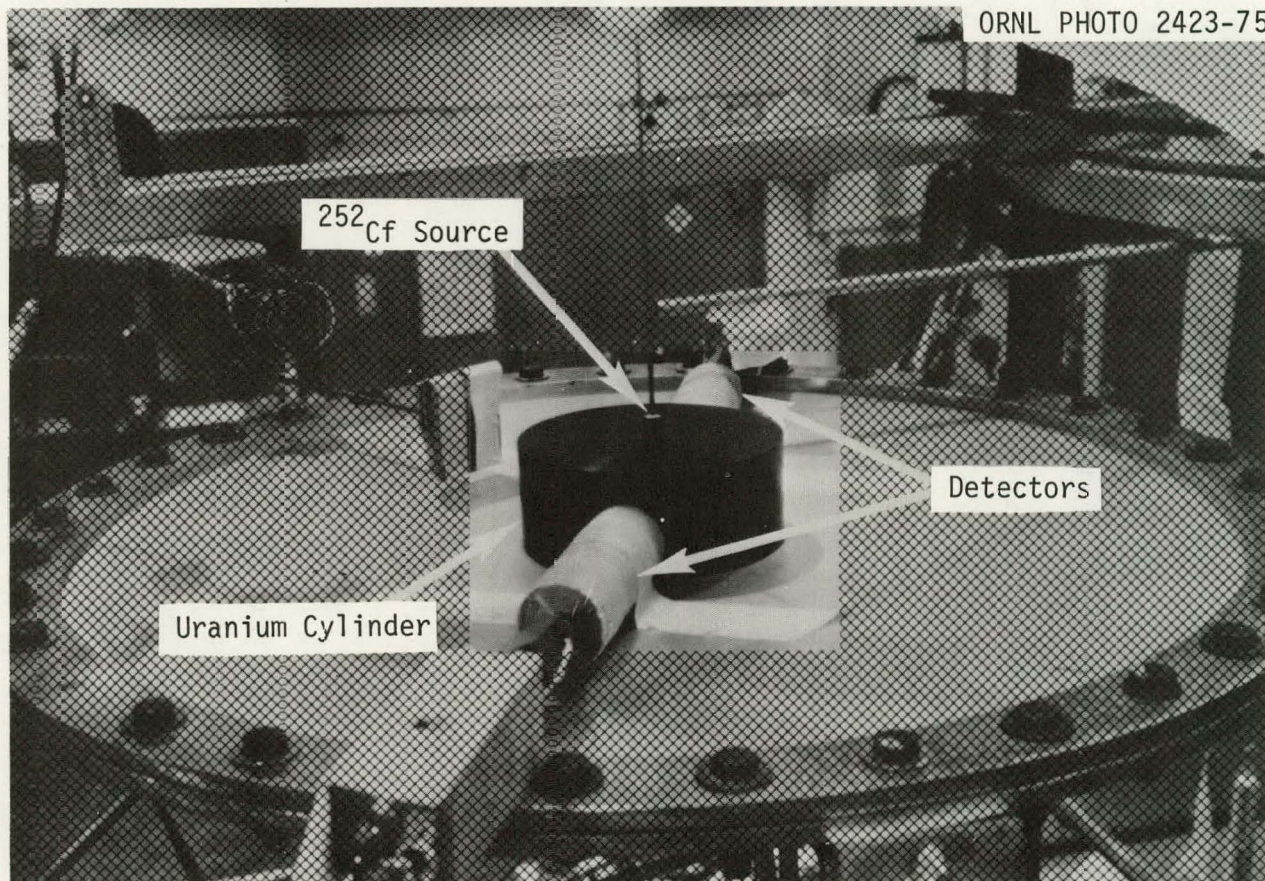
Uranium Cylinder

Fig. 25. Photograph of uranium cylinder showing the location of the detectors and ^{252}Cf chamber.

Table 10. Subcritical reactivity for 17.77-cm-diam
uranium metal cylinders

Height (cm)	Calculated Neutron Multiplication Factor^a	Subcritical Reactivity		
		Calculated $\frac{\Delta k}{k}$ ($\times 10^{-2}$)	Calculated $\frac{\Delta k}{k\beta}$ (dollars)	Measured $\Delta k/k\beta$ (dollars)
12.63	0.9956	0.44	0.67	--
12.22	0.9846	1.56	2.37	2.0
11.59	0.9664	3.48	5.27	5.2
10.80	0.9414	6.22	9.43	9.6
10.18	0.9200	8.71	13.2	13.5
9.23	0.8834	13.20	20.0	20.3
8.28	0.8414	18.81	28.5	28.4

^{a}S_n transport theory calculations using ENDF/B-III data.

5.3 Power Spectral Densities

Since the reactivity of most of the cylinders was considerably
below delayed criticality, the auto- and cross-power spectral densities
were nearly constant up to 100 kHz. This results from the breakfrequency
being >>100 kHz since the prompt-neutron decay constants previously meas-
ured were >10^6 sec^{-1}. The imaginary part of the cross-power spectral
densities with the ^{252}Cf chamber at those frequencies was small (and
thus imprecise) compared to the real part (ratio of the imaginary part
to the real is proportional to ω/α). Thus, the prompt-neutron decay
constant could not be determined satisfactorily from the ratio of the
real to imaginary part of G_{12} due to the frequency limitations of the
Fourier analyzer system.

The measurement time required, which included both data sampling
and minimal processing, was $\sim$20 min for all cylinders, but <1/2 min of
this time was data sampling.

Table 11. Reactivity vs height for
uranium metal cylinders

Cylinder Height (cm)	Reactivity from Prompt-Neutron Decay Constant Measurements[a] (dollars)
12.54	0.08
12.38	0.6
12.07	1.6
11.75	3.1
11.43	4.9
11.11	6.6
10.80	8.2
10.48	10.3
10.16	13.0
9.53	17.0
8.89	22.3
8.26	27.9
7.62	35.0

[a]Obtained from interpolation of reactivity vs cylinder height, where the reactivity was obtained from prompt-neutron decay constant measurements. These reactivities have been corrected for the reflection effect of the detectors, which is ~52 cents.

5.4 Coherence Amplitudes

The spectral densities were combined to form the various coherence functions, and the results for a cylinder with a height of 10.16 cm are shown in Fig. 26. These coherence amplitudes at low frequencies for the various cylinders are plotted as a function of reactivity in Fig. 27. In these measurements (Fig. 27) the ^{252}Cf chamber was operated in the pulse mode and the Li-glass scintillators were used both with and without a lead shield (1.43-cm-thick lead between the uranium cylinder and the detector, and 1.20-cm-thick lead around the sides of the detector). The
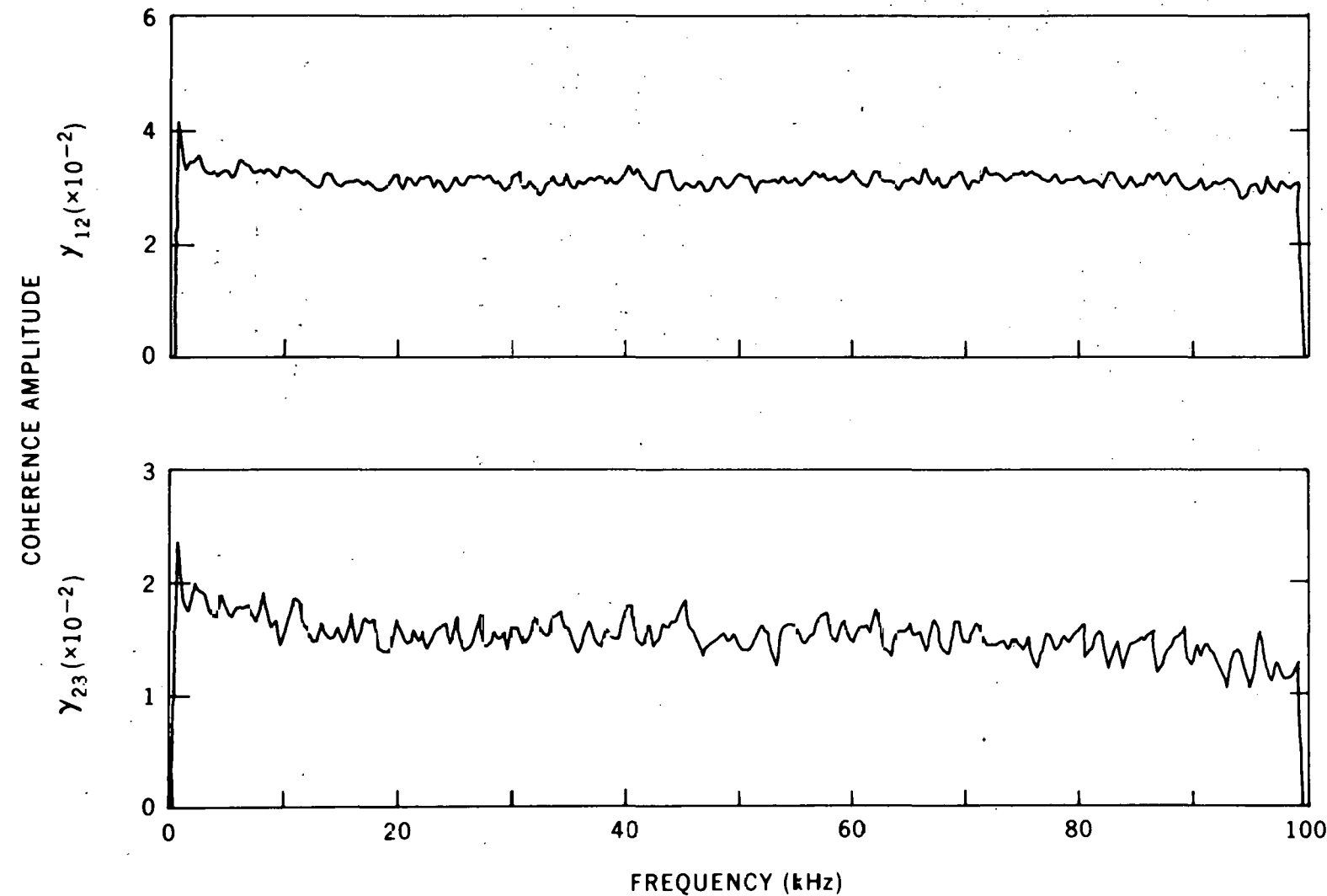
Fig. 26. Coherence amplitudes, γ_{12} and γ_{23}, for the uranium cylinder with a reactivity of 13 dollars subcritical.
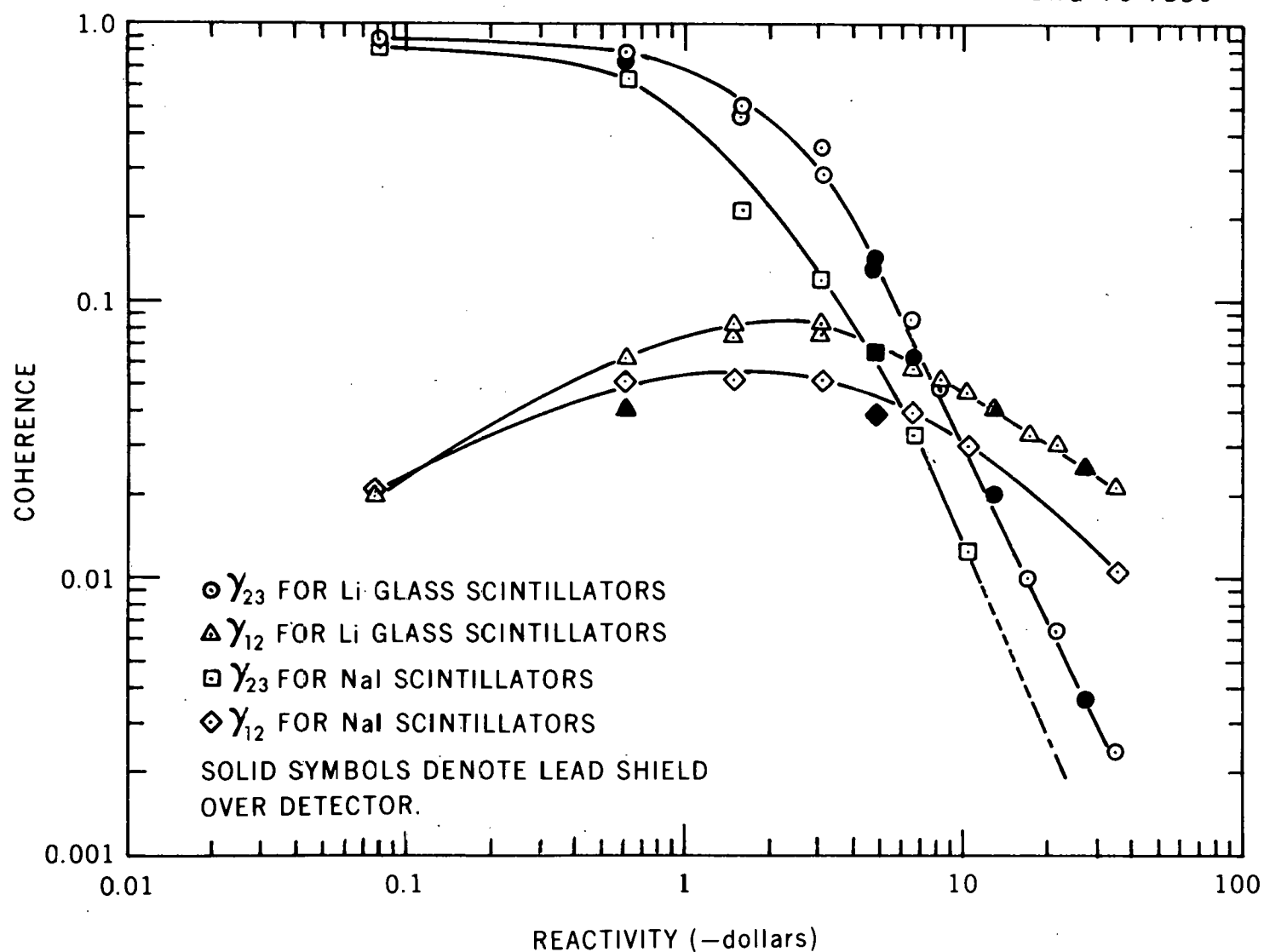
Fig. 27. Coherence amplitude at low frequency as a function of reactivity for 17.77-cm-diam uranium metal cylinders.

values with and without the shield were not very different for the far subcritical cylinders since the decreased detection efficiency (due to the inability to detect some gamma rays and neutrons) was offset by the reduction of the uncorrelated events due to the gamma-ray background from the uranium metal. At reactivities near delayed criticality where the correlated signal is well above the background, the reduced detection efficiency results in a lower value of the coherence amplitude. The coherence amplitudes at low frequency for the measurements with the NaI detectors which were sensitive only to gamma rays (also shown in Fig. 27) are lower than those from the measurements with the glass scintillators because of the lower detection efficiency. The decrease in γ_{12} at low and high reactivity is as predicted by the theory (Fig. 3). Further sub-critical than eight dollars, the cross-power spectral density G_{12} can be measured in a fixed time with Li-glass detectors more precisely than G_{23}. The intersection of the plots of γ_{12} and γ_{23} (Fig. 3) vs reactivity defines a curve of detection efficiency vs reactivity for which the coherence values for these measurements are equal. The experimental coherence values define this subcriticality reactivity as 8 dollars; thus, the detection efficiency is approximately 1.5×10^{-4} count per reactor fission. For less than ~ 0.1 dollar subcritical, theory predicts (Fig. 3) that the coherence will not depend on detection efficiency for $W > 10^{-4}$; this is confirmed by the data of Fig. 27.

5.5 Reactivity from the Ratio $G_{12}^{*}G_{13}/G_{11}G_{23}$

The reactivity determination from the ratio $G_{12}^{*}G_{13}/G_{11}G_{23}$ for the cylinders differs from that for the sphere in that many of the parameters necessary to infer the reactivity were obtained from transport theory calculations rather than from measurements. However, the experimental data available from the sphere measurements has confirmed the validity of the calculational methods.

5.5.1 Value of Y

This ratio was the same as that for the sphere (unity) since there is negligible inherent source in the uranium cylinders.

5.5.2 Value of P_1

Since the pulse mode data were used primarily to obtain the reactivity, P_1 is given by the expression $RXI\bar{\nu}/I_c\bar{\nu}_c$. The number of neutrons per ^{252}Cf fission was obtained as in the interpretation of the sphere measurements. The average number of prompt neutrons per uranium fission was obtained using the fluxes from transport theory calculations[38] and the ENDF/B-III[39] data to calculate the total number of neutrons per uranium fission. The effective delayed-neutron fraction (0.0066) was assumed to be constant with cylinder height and was used to obtain the number of prompt neutrons per fission, which was between 2.600 and 2.608 for cylinder heights between 12.54 and 7.62 cm.

The importance of the neutrons from the spontaneous fission of ^{252}Cf in the ionization chamber, I_c, and the average importance of neutrons from uranium fission, I, were calculated from transport theory calculations. The average importance of neutrons from uranium fission was weighted with the fission density in the cylinders and that for the ^{252}Cf fission neutrons was calculated by including an accurate mock-up of the counter geometry and materials in the transport theory calculation. The ratio of I_c/I for the cylinders varied from 0.610 to 0.755 for cylinder heights varying from 12.54 to 7.62 cm (Fig. 28).

The value of the Diven factor, X, was assumed to be the same as that for the uranium sphere (0.805). The value of the factor R, which accounts for spatial effects in the point kinetics equations, was calculated using the forward and adjoint fluxes from the transport theory calculations (Fig. 29). This calculated factor varied ∿2% for cylinders varying in height from 5 to 12.6 cm. Combining these values, the resulting value of P_1 varied from ∿1.1 to 0.7 with decreasing cylinder height, while P_2, P_3, P_4, and P_5 were approximately constant and approximately equal to 4.5, 5.5×10^{-3}, 1, and 1.4×10^{-2}, respectively.

5.5.3 Reactivity Values

The reactivities obtained from these results are plotted as a function of the reactivity obtained from independent measurements (Table 11) in Fig. 30 for measurements made with Li-glass scintillators or NaI scintillators. The values obtained from $G^*_{12}G_{13}/G_{11}G_{23}$ were generally
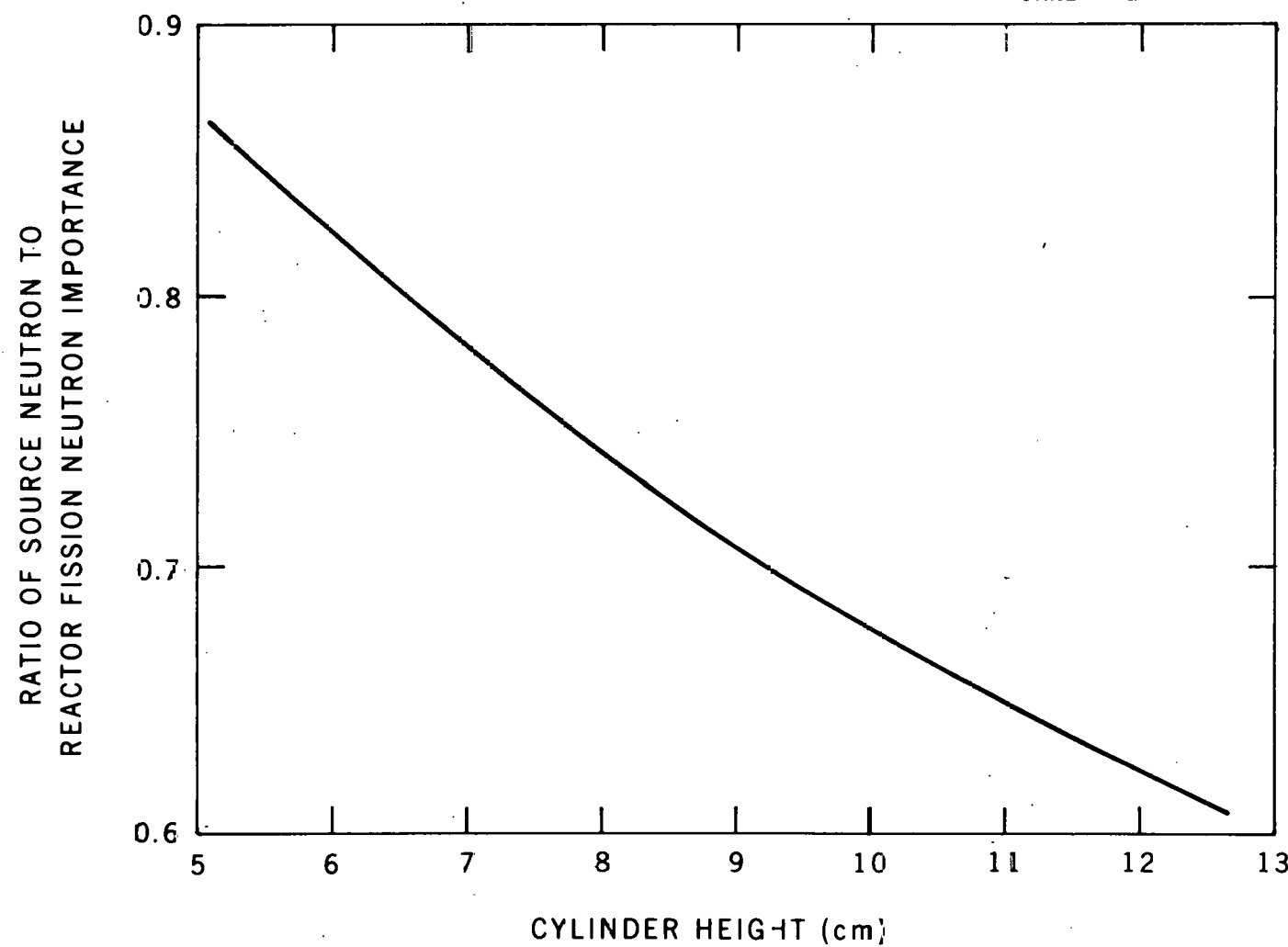
Fig. 28. Ratio of ^{252}Cf neutron importance to reactor fission importance as a function of cylinder height.
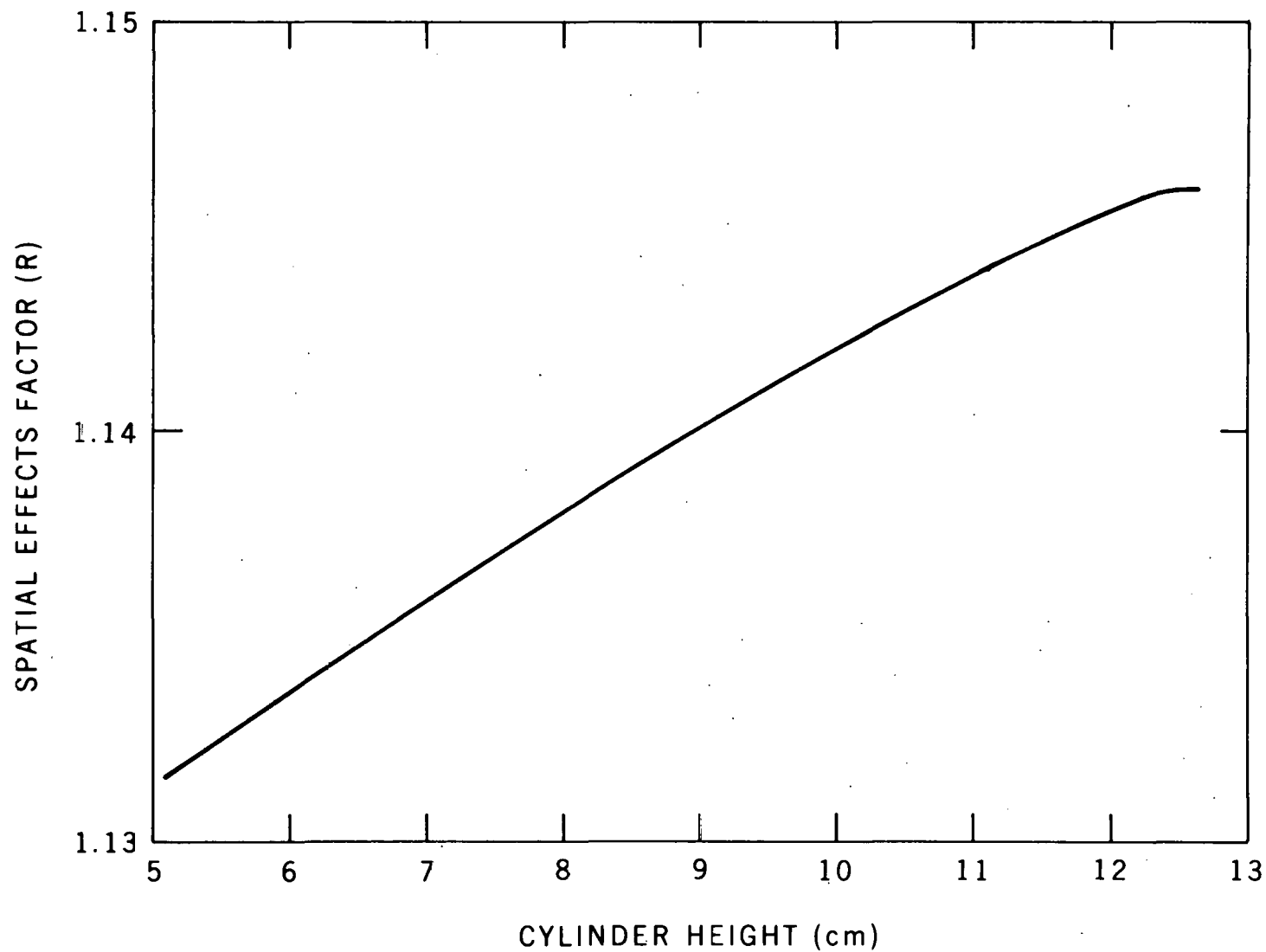
Fig. 29. The spatial effects factor, R, as a function of height for 17.77-cm-diam uranium metal cylinders.
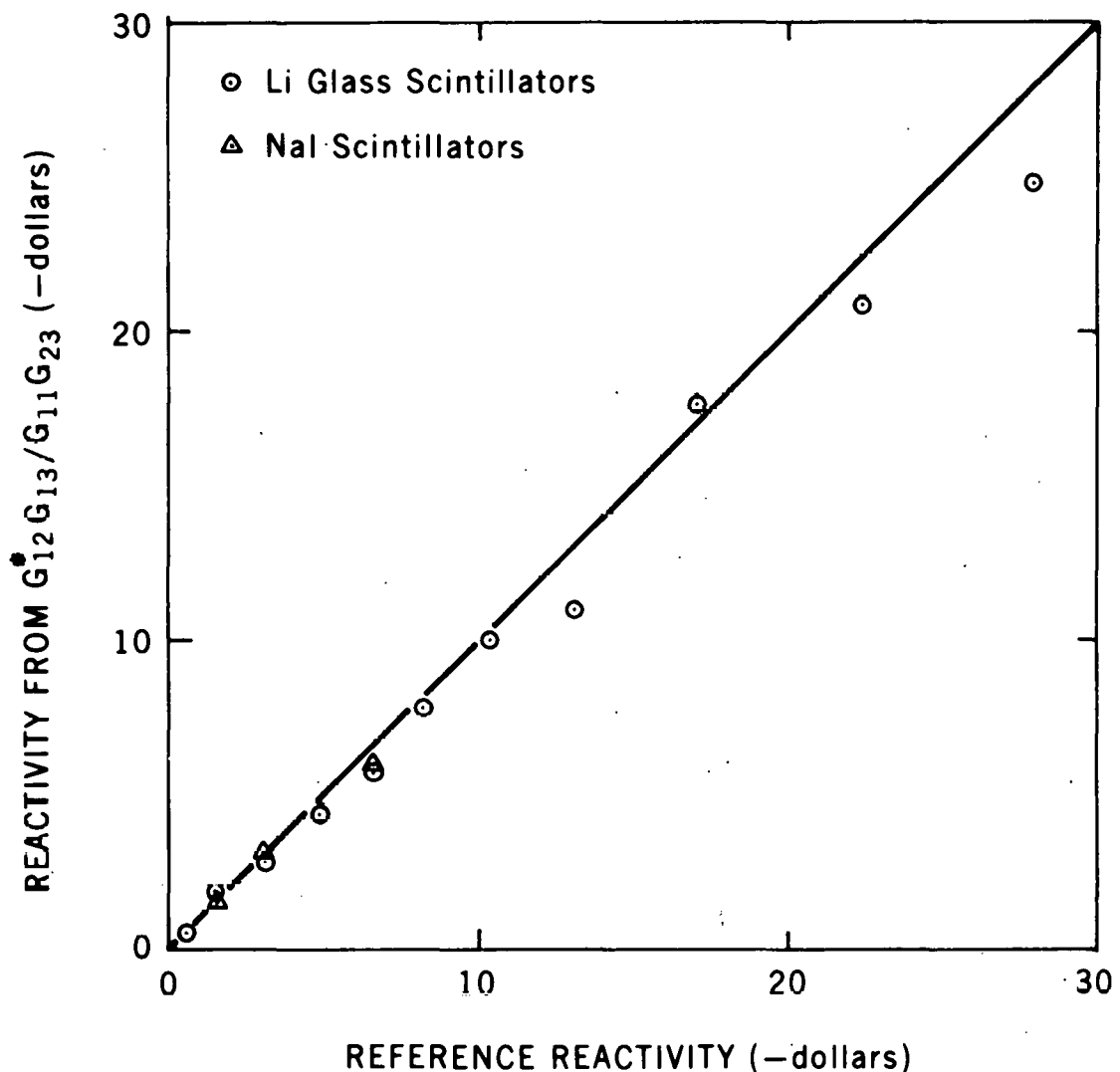
Fig. 30. Comparison of reactivity from $G^*_{12}G_{13}/G_{11}G_{23}$ with reactivity values from other measurements.

slightly lower than the other values, but the agreement with other measurements is good. This demonstrated that this method of reactivity determination is valid for these cylinders down to ~30 dollars subcritical. The reactivity obtained did not depend on the type of detector used, thus demonstrating that the measurement can be performed with a detector sensitive only to gamma rays. Measurements were performed at ~80 dollars subcritical, but the interpretation was not meaningful, probably due to the point kinetic assumptions of the theory.

5.6 Prompt Reactivity From Other Ratios of Spectral Densities

Expressions similar to Eqs. (21) and (22) can be used to obtain the prompt reactivity. The disadvantages of this interpretation are that it requires correction for the frequency response of the instrumentation and a knowledge of the current in the detector in the calibration measurement and in the measurement with the reactor. Two implementations of the two-factor expressions to obtain the prompt reactivity, ρ_p, were used to analyze the data. They are similar in form to Eq. (12) and are as follows:

$$-\rho_p = L_2 \frac{P_1(P_4 - P_5)}{1 - L_2\left(\dfrac{P_1 P_5}{\beta}\right)} , \tag{25}$$

where

$$L_2 = \frac{J_3}{J_{A3}} \text{ Re } \frac{G_{12}^* G_{A13}}{G_{11} G_{23}} , \tag{26}$$

or

$$L_2 = \frac{J_3}{J_{A3}} \frac{\text{Re} G_{c12}}{G_{c23}} \gamma_{A12} \gamma_{A13} . \tag{27}$$

The reactivities obtained using Eqs. (25)-(27) are compared with the reference values in Fig. 31. The values obtained by both methods [Eqs. (26) and (27)] agree. Also, the values do not depend on the detector type or whether the lead shield was present. The values are somewhat lower than the actual values (by as much as 30%) to 30 dollars subcritical. This disagreement is probably due to the inability to accurately measure the current in the measurement with the uranium cylinders. The precision of the current measurement for the subcritical cylinders was low because the current was the sum of a background current from the material (natural gamma activity of the uranium metal) and the current from particles from fission in the uranium metal. The latter component, which is needed for this interpretation of the measurement, was a small part of the total current.

6. CONCLUSIONS

The experiments with the mock-up of the LMFBR confirmed the following theoretical predictions: (a) the imaginary part of G_{12} is negative (Fig. 7); (b) the square of cross-power spectral density, G_{c12} or G_{c13}, can be fitted by a point kinetics theory to obtain a breakfrequency that agrees with those from conventional cross- and auto-power spectral densities, G_{c33} and G_{c23} (Fig. 8); (c) the prompt-neutron decay constant can be obtained from the ratio of the real to the imaginary part of G_{c13} and is constant with frequency, demonstrating the absence of higher mode decay (Fig. 9); (d) the coherence, γ_{12}, between the detector and the ^{252}Cf chamber is not a strong function of reactivity—it varied in the measurement by a factor of only 2 for a reactivity change of almost two decades (Fig. 11); (e) the ratios of spectral densities $\text{Re}G_{c13}\big/\big|G_{c23}\big|$ [Eq. (21)] and $G_{12}^{*}G_{13}/G_{11}G_{23}$ [Eq. (10)] are constant with frequency (Figs. 12 and 13); and (f) the ratio of spectral densities $G_{12}^{*}G_{13}/G_{11}G_{23}$ [Eq. (10)] is independent of detection efficiency—measurements at $\sim$0.8 and $\sim$30 dollars subcritical (Table 1), in which the efficiency was varied by a factor of 100 experimentally by choice of detectors (fission chamber or Li-glass scintillator) or mode of operation (pulse or current) of the
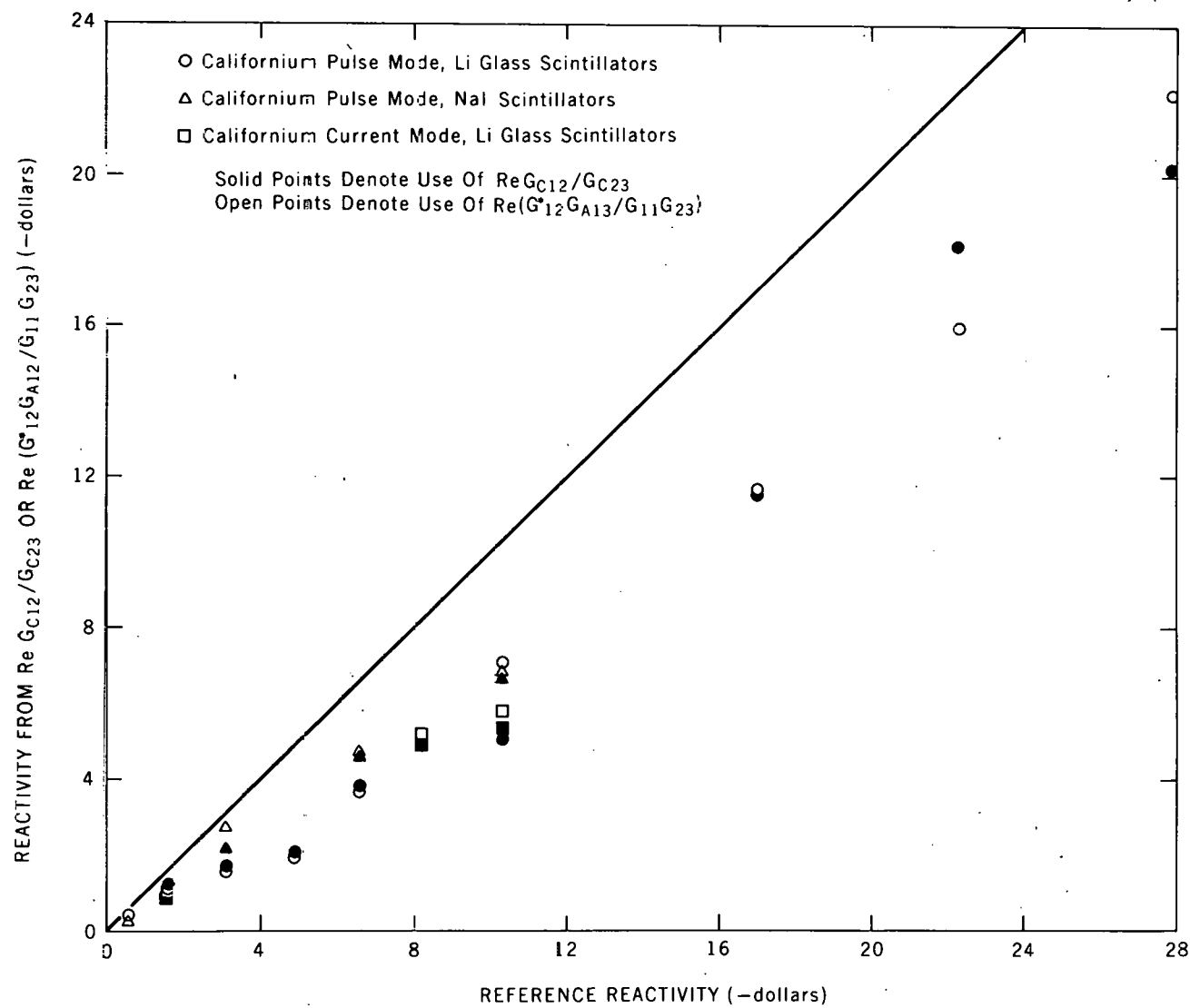
Fig. 31. Comparison of reactivity from $Re(G^*_{12}G_{13}/G_{11}G_{23})$ and ReG_{c12}/G_{c23} with reactivity values from other measurements.

scintillation system, showed the ratio to be independent of detection efficiency.

All predictions of the theory could not be confirmed quantitatively in this experiment because of (a) the inability to determine the terms of Eq. (12) relating to the operation of the chamber containing ^{252}Cf, (b) the inefficiency of the on-line noise analyzer ($\sim$5% sampling time), and (3) the insufficient experimental and preparation time allotted for this first test of this method, 12 days and 6 weeks, respectively.

The experiments with the uranium metal sphere and cylinder, in addition to verifying the above conclusions, demonstrated that (a) the dependence of $G_{12}^{*}G_{13}/G_{11}G_{23}$ on the ratio of total neutron production rate, $F_c I_c \bar{\nu}_c + F_i I_i \bar{\nu}_i$ (from the ^{252}Cf source and an inherent source), to the neutron production rate, $F_c I_c \bar{\nu}_c$, from the ^{252}Cf source was linear as predicted by Eq. (11); (b) the value of $B_c(1 + C_\alpha)$ could be obtained from measurements in which the ^{252}Cf chamber was operated in the pulse and current modes and $\overline{\nu_c^2}/\bar{\nu}_c^2$ could be measured by this method; (c) the measurement of $\overline{\nu_c^2}/\bar{\nu}_c^2$ by the ^{252}Cf spectral density method provides an ideal check on the detection system, and the accuracy of the Fourier analyzer processing (both hardware and software) systems; (d) the ratio of spectral densities $G_{12}^{*}G_{13}/G_{11}G_{23}$ was used successfully to obtain the reactivity down to about 30 dollars subcritical; and (e) reactivity interpretations which required measurement of the detector current were not satisfactory because of the inability to measure the current from interactions with particles from fission events in the presence of a high background current from the natural activity of the uranium metal.

These measurements demonstrate the feasibility of the determination of the reactivity from the ratio of spectral densities $G_{12}^{*}G_{13}/G_{11}G_{23}$ for fast uranium and plutonium systems down to neutron multiplication factors of 0.8. The new methods of reactivity determination enable the determination of subcriticality without a knowledge of the properties of the reactor or critical assembly at delayed criticality. In this method the interpretation of the measured data to obtain the reactivity does not depend on the relative or absolute values of the reactor inherent source intensity or the detection efficiency. Since these methods do not require

calibration at a known reactivity state, they can be used in the initial loading of a reactor where subcriticality determination cannot depend on some calibration near delayed criticality. They also may be useful in determining the reactivities of assemblies where sufficient material to achieve criticality is not available or where loading to criticality is undesirable. This method has potential use in the startup of LMFBRs to determine the reactivity far subcritical before initial criticality is approached and could be used in the initial startup of FFTF with in-core detectors to obtain the reactivity as fuel is loaded into the outer two rows of the core.

THIS PAGE

WAS INTENTIONALLY

LEFT BLANK

REFERENCES

1. J. T. Mihalczo, *Nucl. Sci. Engr.* <u>41</u>, 296 (1970); also J. T. Mihalczo, "Use of ^{252}Cf as a Randomly Pulsed Neutron Source for Prompt Neutron Decay Measurements," Y-DR-41, UCC-ND Oak Ridge Y-12 Plant (1970).

2. J. T. Mihalczo and V. K. Paré, "Theory of Correlation Measurements in Time and Frequency Domains with ^{252}Cf," ORNL/TM-4732, Oak Ridge National Laboratory (November 1974).

3. V. K. Paré and J. T. Mihalczo, "Reactivity from Power Spectral Density Measurements with Californium-252," *Nucl. Sci. Engr.* <u>56</u>, 213-218 (1975).

4. J. T. Mihalczo and V. K. Paré, "Theory of Correlation Measurement in Time and Frequency Domains with ^{252}Cf," *Annals of Nuclear Energy* <u>2</u>, 97-105 (1975).

5. J. T. Mihalczo, V. K. Paré, and M. V. Mathis, "Power Spectral Density Measurements with ^{252}Cf for a Mockup of the FFTF," *Trans. Amer. Nucl. Soc.* <u>21</u>, 449-450 (June 1975).

6. J. T. Mihalczo, G. L. Ragan, and G. C. Tillett, "Power Spectral Density Measurements with ^{252}Cf for Unreflected Uranium (93.2 wt % ^{235}U) Metal Sphere," *Trans. Amer. Nucl. Soc.* <u>22</u>(1), 691 (June 1975).

7. J. T. Mihalczo, G. L. Ragan, and G. C. Tillett, "Power Spectral Density Measurements with ^{252}Cf for Unreflected 17.77-cm-diam Uranium (93.2 wt % ^{235}U) Metal Cylinders," *Trans. Amer. Nucl. Soc.* <u>23</u>, 521 (June 1976).

8. M. Otsuka and T. Iijima, *Nucleonik* <u>7</u>(8), 488 (1965).

9. D. R. Harris, *Nucl. Sci. Engr.* <u>21</u>, 369 (1965).

10. G. I. Bell, *Nucl. Sci. Engr.* <u>21</u>, 390 (1965).

11. J. E. Werle, C. B. McGough, P. A. Edwards, and A. Selz, *Nucl. Eng. Int.* <u>17</u>, 617 (August 1972).

12. R. C. Kryter, ORNL, personal communication (1973).

13. W. Seifritz, "Ein On-Line Reaktivitätsmeter für Schnelle Reaktoren mit Hilfe von Cf-252 Neutronen Reaktortagund," Bonn (1971).

14. R. W. Badgley and R. E. Uhrig, *Nucl. Sci. Engr.* <u>19</u>, 158-163 (1964).

15. C. E. Cohn, *Nuc. Sci. Engr.* <u>7</u>, 472 (1960).

16. W. Seifritz, "Die Bestimmung von Kinetischen Reaktorparametern durch die Polaritätskor relation des Neutronenrauschens im Frequenzbereich," doctoral dissertation, INR-4109-24, Kernforschungszentrum Karlsruhe (February 1969).

17. G. M. Hess and R. W. Albrecht, "Polarity Spectral Analysis Reactivity Errors," *Trans. Amer. Nucl. Soc.* 12, 738 (1969).

18. N. J. Ackermann, Jr., and A. R. Buhl, "The Detection Efficiency Dependence of Subcriticality Measurements by the Polarity Spectral Coherence Measurement," *Nucl. Technol.* 12, 320 (1971).

19. J. F. Walter, *Nucl. Appl.* 3, 271 (May 1967).

20. N. J. Ackermann, Jr., "Subcriticality Measurement in an LMFBR," *Nucl. Saf.* 12, 507 (1971).

21. J. T. Mihalczo, *Nucl. Sci. Eng.* 41, 296 (1970).

22. J. T. Mihalczo, *Nucl. Sci. Eng.* 46, 147 (1971).

23. J. T. Mihalczo, *Nucl. Sci. Eng.* 60, 262 (1976).

24. W. Y. Kato, G. K. Reisch, L. R. Dates, A. E. Till, A. Ancaroni, J. Van Doorninck, C. L. Cheever, and E. M. Bohm, "The Final Safety Analysis Report on the Use of Plutonium in ZPR-6 and -9," ANL-7442 (February 1970).

25. Letter, A. Travelli to R. A. Bennett, "Detailed Plans for the FFTF-EMC Experiments; Phase D parts I and II," Argonne National Laboratory (Dec. 15, 1972).

26. M. V. Mathis, J. T. Mihalczo, V. K. Paré, "Reactivity Surveillance Instrumentation for Measurements with tho FFTF Engineeriug Muck-Up Core," ORNL/TM-4511 (1976).

27. J. T. Mihalczo, M. V. Mathis, V. K. Paré, "Reactivity Surveillance Procedures Experiments with the FFTF Engineering Mockup Core," ORNL/TM-4704 (May 1976).

28. J. T. Mihalczo, M. V. Mathis, V. K. Paré, "Reactivity Surveillance Experiments with the Engineering Mock-up Core of the Fast Flux Test Facility Reactor," *Nucl. Sci. Engr.* 59, 350-368 (1976).

29. V. K. Paré, R. C. Kryter, and J. T. Mihalczo, "Experience with a Digital Noise Analysis System in Subcriticality Measurements on a Mock-Up of the FFTF," *Proc. Nucl. Sci. Symp.* NS-21(1), 767 (1974).

30. J. T. Mihalczo, G. C. Tillett, D. Selby, "Evaluation of Initial Loading Count Rate Data for the FFTF from Critical Experiments with a Mock-Up Core," ORNL/TM-5106 (March 1976).

31. J. T. Mihalczo, "Time Domain Noise Measurements for Fast Metal Assemblies with ^{252}Cf," *Annals of Nuclear Energy* 2, 161-175 (1975).

32. E. R. Rohrer et al., *Neutron Physics Division Annual Progress Report, September 1, 1961*, ORNL-3193, Oak Ridge National Laboratory (1961).

33. J. Allen, ORNL, personal communication (1975).

34. J. W. Boldeman, "Prompt-Neutron Yield from the Spontaneous Fission of Californium-252," *Nucl. Sci. Engr.* 55, 188 (1974).

35. J. T. Mihalczo, "Neutron Importance and Fission Density in Uranium-234-Enriched Uranium and Plutonium Metal Spheres," *Nucl. Sci. Engr.* 56, 271-290 (1975).

36. A. DeVolpi, "Discrepancies and Possible Adjustments in the 220 m/s Fission Parameters," ANL-7830, Argonne National Laboratory (1971).

37. S. Cox, P. Fields, A. Friedman, R. Sjoblom, and A. Smith, *Phys. Rev.* 112, 960 (1958).

38. W. W. Engle, Jr., "A User's Manual for ANISN," K-1693, Oak Ridge Gaseous Diffusion Plant (1967).

39. ENDF/B-III Tape 986 distributed by the National Cross Section Center, Brookhaven National Laboratory (1971).

40. G. R. Keepin, T. F. Wimmett, and R. K. Zeigler, *Phys. Rev.* 107, 1044 (1957).

41. C. F. Masters, M. M. Thorpe, and D. B. Smith, *Nucl. Sci. Engr.* 36, 202 (1969).

42. M. S. Krick and A. E. Evans, *Nucl. Sci. Engr.* 47, 311 (1972).

43. R. Bachelor and H. R. McKhyder, *J. Nucl. Energy* 3, 7 (1956).

44. B. C. Diven et al., *Phys. Rev.* 101, 1012 (1956).

45. J. T. Mihalczo, *Nucl. Sci. Engr.* 32, 292-301 (1968).

46. J. T. Mihalczo, *Nucl. Sci. Engr.* 20, 60 (1964).

THIS PAGE

WAS INTENTIONALLY

LEFT BLANK

ORNL/TM-5475
Dist. Category UC-79, -79d,
-79e, -79m, and -79p

INTERNAL DISTRIBUTION

1.	N. J. Ackermann, Jr. (consultant)	39-48.	V. K. Paré
2.	J. W. Allen	49.	R. B. Perez
3-7.	R. S. Booth	50.	L. M. Petrie
8.	J. F. Ellis	51-55.	G. L. Ragan
9.	G. F. Flanagan	56.	C. W. Ricker
10.	D. N. Fry	57.	E. R. Rohrer
11.	L. B. Holland	58.	J. C. Robinson (consultant)
12.	J. D. Jenkins	59.	G. S. Sadowski
13.	E. B. Johnson	60.	D. Selby
14.	T. W. Kerlin (consultant)	61.	F. Shahrokhi
15.	R. C. Kryter	62.	W. H. Sides, Jr.
16.	J. J. Lynn	63.	J. R. Taylor
17.	D. W. Magnuson	64.	J. T. Thomas
18.	F. C. Maienschein	65-69.	G. C. Tillett
19.	J. D. McLendon	70.	C. R. Weisbin
20.	W. T. Mee	71.	G. E. Whitesides
21-35.	J. T. Mihalczo	72-73.	Central Research Library
36.	J. E. Mott (consultant)	74.	Document Reference Section
37.	F. R. Mynatt	75-77.	Laboratory Records Department
38.	L. C. Oakes	78.	Laboratory Records, ORNL R.C.
		79.	ORNL Patent Office

EXTERNAL DISTRIBUTION

80-81. Director, Division of Reactor Development and Demonstration, Energy Research and Development Administration, Washington, D. C. 20545

82. Director, Reactor Division, Oak Ridge Operations Office, P. O. Box E, Oak Ridge, TN 37830

83. Research and Technical Support Division, ERDA, ORO

84-373. Given distribution as shown in TID-4500 for categories UC-79, -79d, -79e, -79m, and -79p